ACIBADEM MEHMET ALI AYDINLAR UNIVERSITY
INSTITUTE OF HEALTH SCIENCES

INVESTIGATION OF THE EFFECTS OF MITOCHONDRIA TARGETED DRUG LOADED NANOPARTICLES ON COLON CANCER

AYŞEGÜL EKMEKÇİOĞLU

PH.D. THESIS

DEPARTMENT OF MEDICAL BIOTECHNOLOGY

SUPERVISOR
Prof. Meltem Müftüoğlu

ISTANBUL - 2024

ACIBADEM MEHMET ALI AYDINLAR UNIVERSITY
INSTITUTE OF HEALTH SCIENCES

INVESTIGATION OF THE EFFECTS OF MITOCHONDRIA TARGETED DRUG LOADED NANOPARTICLES ON COLON CANCER

AYŞEGÜL EKMEKÇİOĞLU

PH.D. THESIS

DEPARTMENT OF MEDICAL BIOTECHNOLOGY

SUPERVISOR
Prof. Meltem Müftüoğlu

ISTANBUL - 2024

DECLARATION

I declare that this thesis work is my own work, I had no unethical behavior at any stages from the planning to the writing of the thesis, I obtained all the information in this thesis in accordance with academic and ethical rules, I cited all the information and comments that were not obtained with this thesis work, and I provided resources in the list of references. I also declare that there was no violation of any patents and copyrights during the study and writing of this thesis.

06.06.2024
Ayşegül EKMEKÇİOĞLU

PREFACE AND ACKNOWLEDGEMENT

As I am completing my doctorate at Acıbadem Mehmet Ali Aydınlar University, I would like to express my appreciation. Primordially, I am grateful for my thesis advisor, Prof. Meltem Müftüoğlu; who never spared her unwavering support and wisdom, and encouraged me to proceed with my doctorate journey. Her expertise and knowledge have been pivotal in refining this research. I am also thankful to Assist. Prof. Özgül Gök Özatay and Assoc. Prof. Sedef Erdal for devoting their valuable time to me with their valuable feedback and contributions. This study was supported by the Scientific and Technological Research Council of Turkey (TUBITAK), grant no: 119Z249. I would like to thank TUBITAK for its support and Acıbadem Mehmet Ali Aydınlar University for providing us with world-standard laboratories and opportunities.

My lab-mate İlayda Darılmaz; whom I discuss every experiment dilemma with; is my bundle of joy with her presence. İrem Mine Çakır; our chronic intern; who never left us in any condition and also assisted us profoundly. I am also grateful to my old fellow colleagues Tuğçe Ertüzün and Berna Somuncu for promoting me to start my journey as a doctorate student. Also, I owe all my precious fifth-floor colleagues a debt of gratitude. Lastly, I want to express my gratefulness to my friends who stand by me since university. They are my main source of bliss and fortune in my academic life. I thank my dearest companion Ece Aksoy for boosting me with her whimsical character and being my faithful reminder to take breaks. Gizem Şele, with her witty remarks, is my sunshine during moody days. Gülin Baran, who always help me, is my scientific support through this journey.

Ultimately, I would like to deeply appreciate my mother Özlenen Ekmekçioğlu, my father Melih Ekmekçioğlu, and my sister Zeynep Ekmekçioğlu for their endless endorsement, moral, and tolerance of my both physical and emotional absence. Once for all, I would like to thank my dearest sister; who gave me logistical support on this path unconditionally. None of this would have been possible without their encouragement.

TABLE OF CONTENTS

LIST OF ABBREVIATIONS AND SYMBOLS

5-FU	5-fluorouracil
18:0 PEG$_{2000}$ PE	1,2-distearoyl-sn-glycero-3-phosphoethanolamine-N-[methoxy(polyethylene glycol)-2000] (ammonium salt)
^{1}H-NMR	Proton nuclear magnetic resonance
A549	Lung cancer cell line
CCK-8	Cell counting kit 8
$CDCl_3$	Chloroform
Chol	Cholesterol
CI	Cell index
CO_2	Carbon dioxide
COLO205	Human Caucasian colon adenocarcinoma cell line
DCF	2',7'-dichlorofluorescein
DCM	Dichloromethane
ddH_2O	Double distilled water
$\Delta\Psi_m$	Membrane potential of mitochondria
$\Delta\Psi_p$	Membrane potential of plasma
DLC	Delocalized lipophilic cation
DLS	Dynamic light scattering
DMEM	Dulbecco's modified eagle medium
DOPE	1,2-dioleoyl-sn-glycero-3-phosphoethanolamine
Dox	Doxorubicin HCl
Dox-loaded PPL	Doxorubicin-loaded PEG-PE liposome
Dox-loaded TPPL	Doxorubicin-loaded TPP-PEG-PE liposome
DPBS	Dulbecco's phosphate buffer saline
DQA	Dequalinum
DSPE-PEG$_{2000}$-NH_2	1,2-distearoyl-sn-glycero-3-phosphoethanolamine-N-[amino(polyethylene glycol)-2000] (ammonium salt)
ECM	Extracellular matrix
EDCI	N-(3-dimethylaminopropyl)-N′-ethylcarbodiimide hydrochloride

Em	Emission
EPR	Enhanced permeability and retention
EtOH	Ethanol
Ex	Excitation
FBS	Fetal bovine serum
FDA	Food and Drug Administration
h	Hour
H_2DCFDA	2',7'-dichlorodihydrofluorescein diacetate
HCT116	Human colorectal carcinoma 116 cell line
Hsp70	Heat shock protein 70
HT-29	Human colon adenocarcinoma cell line
IC_{50}	Half-maximal inhibitory concentration
IMM	Inner mitochondrial membrane
IMS	Intermembrane space
i.v.	Intravenously
kDa	Kilodalton
λ_{max}	Lambda max
L-α-PC	L-α-Phosphatidylcholine from egg yolk
Log P	Partition coefficient
MDA-MB-231	Human breast adenocarcinoma cell line
µL	Microliters
mL	Milliliters
µM	Micromolar
min	Minutes
MLV	Multilamellar vesicle
mM	Millimolar
MPP	Mitochondria-penetrating peptide
MTG	Mitotracker green
MTS	Mitochondria-targeting sequence
mV	Millivolt
MVL	Multivesicular liposome
MWCO	Molecular weight cut off

NAC	N-Acetyl cysteine
NaCl	Sodium chloride
NHS	N-hydroxysuccinimide
nm	Nanometer
nM	Nanomolar
OD	Optical density
OLV	Oligolamellar vesicle
OMM	Outer mitochondrial membrane
PA	Phosphatidic acid
PBS	Phosphate buffer saline
PC	Phosphatidylcholine
PDI	Polydispersity index
PE	Phosphatidylethanolamine
PEG	Polyethylene glycol
PES	Polyethersulfone
Pen/Strep	Penicillin/Streptomycin
PG	Phosphatidylglycerol
PI	Phosphatidylinositol
pKa	Dissociation constant
PPL	Empty PEG-PE liposome
ppm	Parts per million
PS	Phosphatidylserine
Redox	Oxidation reduction
Rh 123	Rhodamine 123
RhB, RhB DHPE	Rhodamine B 1,2-dihexadecanoyl-sn-glycero-3 phosphoethanolamine, triethylammonium salt
RhB-PPL	Rhodamine B-labeled PEG-PE liposome
RhB-TPPL	Rhodamine B-labeled TPP-PEG-PE liposome
ROS	Reactive oxygen species
RT	Room temperature
SS	Szeto-Schiller
STD	Standard deviation

STPP	Stearyl triphenylphosphonium
TAIII	Timosaponin AIII
TEA	Triethylamine
TEM	Transmission electron microscopy
TME	Tumor microenvironment
TMS	Tetramethyl silane
TPP	Triphenylphosphonium, (3-carboxypropyl) triphenylphosphonium bromide
TPPL	Empty TPP-PEG-PE liposome
ULV	Unilamellar vesicle
WST-8	Water soluble tetrazolium-8

LIST OF FIGURES

LIST OF TABLES

ABSTRACT

Investigation of the Effects of Mitochondria Targeted Drug Loaded Nanoparticles on Colon Cancer

In this thesis study, mitochondria-targeted (DSPE-PEG-TPP polymer conjugated) liposomes were developed to improve the therapeutic index of chemotherapeutic agents that function in mitochondria, potentially leading to reduced side effects. Doxorubicin (Dox) loaded mitochondria-targeted liposomes (TPPL) and non-targeted PEGylated liposomes (PPL) were compared based on physicochemical properties, morphology, release profile, cellular uptake, mitochondrial localization, and anticancer effects. All formulations were spherically shaped with appropriate size, dispersity, and zeta potential. The stability of the empty liposomes was favorable for two months at 4 °C. Confocal microscopy results demonstrated that TPPL were co-localized in mitochondria, but, no localization was observed for PPL. The release kinetics of Dox-loaded liposomes showed that Dox released from TPPL was higher at pH 5.6 than at pH 7.4, which indicates a higher accumulation of the released drug in the tumor microenvironment. All empty liposomes were not cytotoxic to HCT116 cells even at high concentrations. The half-maximal inhibitory concentration of Dox-loaded TPPL and PPL was 1.62-fold and 1.17-fold lower than that of free Dox, respectively. Moreover, the reactive oxygen species level was significantly increased when HCT116 cells were treated with Dox-loaded TPPL. In conclusion, since the special bilayer structure of mitochondrion is a potential therapeutic target in the diagnosis and treatment of diseases such as cancer, DSPE-PEG-TPP polymer conjugated liposomes may be promising for targeted drug delivery to mitochondria.

Keywords: mitochondria-targeted liposomes, doxorubicin hydrochloride, drug release, cytotoxicity, colon cancer

ÖZET

Mitokondriye Hedefli İlaç Yüklü Nanoparçacıkların Kolon Kanseri Üzerine Etkilerinin Araştırılması

Bu tez çalışmasında, mitokondriye hedefli (DSPE-PEG-TPP polimer konjuge edilmiş) lipozomlar, mitokondride işlev gören kemoterapötik ajanların terapötik indeksini iyileştirmek ve potansiyel yan etkilerinin azaltılması için geliştirildi. Doksorubisin (Dox) yüklü mitokondriye hedefli lipozomlar (TPPL) ve hedeflenmemiş PEG kaplı lipozomlar (PPL), fizikokimyasal özellikleri, morfolojisi, salım profili, hücresel alımı, mitokondriyal lokalizasyonu ve antikanser etkilerine göre karşılaştırıldı. Tüm formülasyonların uygun boyut, dağılım ve zeta potansiyeli ile birlikte küresel şekilli olduğu saptandı. Boş lipozomların stabilitesini 4 °C'de iki ay boyunca koruduğu gözlemlendi. Konfokal mikroskopi sonuçlarına göre TPPL'nin mitokondride lokalize olduğu gösterilirken PPL için herhangi bir lokalizasyon gözlemlenmedi. Dox yüklü lipozomların salım kinetiği sonucuna göre, pH 5.6'da TPPL'den salınan Dox'un pH 7.4'e göre daha yüksek çıkması ile lipozomdan salınan ilacın tümör mikroçevresinde birikiminin daha yüksek olduğu gösterildi. Boş lipozomların tümü, yüksek konsantrasyonlarda bile HCT116 hücrelerine karşı sitotoksisite göstermedi. Dox yüklü TPPL ve PPL'nin yarı maksimum inhibitör konsantrasyonlarının, serbest Dox'a göre sırasıyla 1.62 kat ve 1.17 kat daha düşük olduğu gösterildi. Ayrıca, HCT116 hücreleri Dox yüklü TPPL ile muamele edildiğinde reaktif oksijen türleri seviyesi önemli ölçüde arttığı bulundu. Sonuç olarak, mitokondrinin özel çift tabakalı yapısı, kanser gibi hastalıkların tanı ve tedavisinde potansiyel bir terapötik hedef olduğundan, DSPE-PEG-TPP polimeri konjuge edilmiş lipozomlar, mitokondriye hedefe yönelik ilaç dağılımı için umut verici olabilir.

Anahtar Sözcükler: mitokondriye hedefli lipozomlar, doksorubisin hidroklorür, ilaç salımı, sitotoksisite, kolon kanseri

1 INTRODUCTION AND AIM

Many studies showed that the properties of the anticancer drugs known to be effective on intracellular organelles became more advantageous when encapsulated into a nanocarrier system. For instance, there are lots of studies based on mitochondria targeting which provides more stable molecules with enhanced therapeutic effects for both *in vivo* and *in vitro*. Also, the nanocarrier systems minimize the side-effects of free drugs alone. Zhou et al. showed that paclitaxel encapsulated into mitochondria-targeting liposome inhibited lung cancer xenograft tumor growth ~50% more than free paclitaxel (1). Another study remarked that 5-fluorouracil (5-FU) loaded liposomes including the tumor targeting group on it were less cytotoxic to the colon cancer cells (HT-29) than free 5-FU (2). Additionally, since the plasma half-life of 5-FU (15-20 min) is low, the therapeutic dosage can only be reached by using very high amounts of the drug. Encapsulation of 5-FU also provides enhanced stability, and circulation time, and decreases the tumor growth with lower doses of 5-FU (2,3).

Liposomes are the most preferred nanocarrier systems for cancer treatment due to their biocompatibility, non-toxicity, biodegradability, targeted drug delivery and release, increased therapeutic effect, and decreased side effects (4). The stability of liposomes can be increased by adding polyethylene glycol (PEG) which is mostly used in hydrophilic and biocompatible polymeric structures. PEG chains also prevent aggregate formation by interacting with blood constituents, and macrophage uptake, and increase blood circulation time. Solid tumors of colon, breast, lung, and prostate cancers have increased vascular permeability and destroyed lymphatic drainage when compared to healthy tissues. This property of cancerous tissues makes them permeable to nano-scaled particles like liposomes. This type of targeting of nanocarriers is known as passive targeting (4–8).

The metabolic stability of every drug molecule is not the same with each other. Therefore, in order to enhance the therapeutic effect of the drug molecule known to be effective on intracellular organelles (like mitochondria) the effective site of the cell should be targeted by using targeting group involving nanocarriers (9,10).

Mitochondria have key roles in both cell proliferation and death. Therefore, it is an important intracellular organelle as a target for anticancer drugs. The idea of targeting mitochondria depends on the difference between the mitochondrial membrane potential (-180 mV) and the plasma membrane which is much higher than the mitochondrial membrane potential. Also, the amount of mitochondria in cancer cells is much more higher than in normal epithelial cells. Since tumor cells have highly negative membrane potential, lipophilic cations like triphenylphosphonium (TPP), dequalinum (DQA) and rhodamine 123 (Rh 123) will selectively accumulate more at the mitochondria of cancer cells compared to normal cells (10,11).

To sum up, the main aim of this thesis was to load Dox into both non-targeted and mitochondria-targeted liposomal formulations. As mentioned before, liposomes could go through the body and function like a vehicle that can reach the specific tissue, organ, or receptor of interest. This was done by adding molecules on the liposome surface that function like molecular “keys”. To achieve that, TPP and PEG were included as physicochemical properties to the liposomal formulation as mitochondria-targeting conjugate and for increasing the stability of the liposome, respectively. By this manner, reduced toxicity was aimed while maintaining or improving treatment efficacy. Due to the adjusted liposomal formulation, it was expected that the encapsulated drug molecule would be released at mitochondria and thereby the therapeutic effect of the drug would be enhanced. Additionally, the random interactions of the drug with other organelles would be prevented and therefore off-target effects would be reduced. Furthermore, they can be used as monotherapy or combined therapy for various cancers. The mitochondria-targeted liposomes to be prepared in this project might have the potential to be used in targeting different types of cancer and mitochondrial diseases.

2 BACKGROUND

2.1 Use of Liposomes as Nanocarriers

In the mid-1960s, a British hematologist Alec D. Bangham, and his colleague R.W. Thorne from the Babraham Institute of Cambridge University managed research about liposomes. During this journey of liposomes, Bangham observed “onion-like” structures which belonged to phospholipids under the electron microscope (12,13). Bangham got inspired by his surname at first and named those structures “Banghasomes”. However, Bangham’s close friend Gerald Weissmann became the eponym of those structures and proposed the word “liposomes” which originally came from the combination of two Greek words “lipos” and “soma” which can be defined as fat and body, respectively (14,15). According to Weismann’s definition, liposomes are described as “microscopic vesicles composed of one or more lipid bilayers”. Basically, liposomes are spherically shaped structures composed of a lipid bilayer membrane with an aqueous core. Due to their structures, liposomes have the ability to encapsulate both hydrophilic and hydrophobic molecules (16,17).

Liposomes are the most preferred nanocarrier systems for cancer treatment due to their biocompatibility, non-toxicity, biodegradability, ability to self-assembly, targeted drug delivery, and release, increased therapeutic effect, and decreased side-effects (4,18).

2.1.1 Classification of liposomes

Liposomes are classified in various properties like their size, number of bilayers, composition, and preparation methodology (19).

2.1.1.1 Based on structure

Depending on the size and number of bilayer liposomes divided into four as unilamellar vesicles (ULVs), oligolamellar vesicles (OLVs), multilamellar vesicles

(MLVs), and multivesicular liposomes (MVLs) (Figure 1). As the name implies ULVs are composed of single-lipid bilayer with a diameter of 20-250 nm whereas OLVs and MLVs include two or more lipid bilayers of 1-5 μM (19–21). The structure of MVLs consists of non-concentric aqueous chambers surrounded by a single phospholipid bilayer (21).

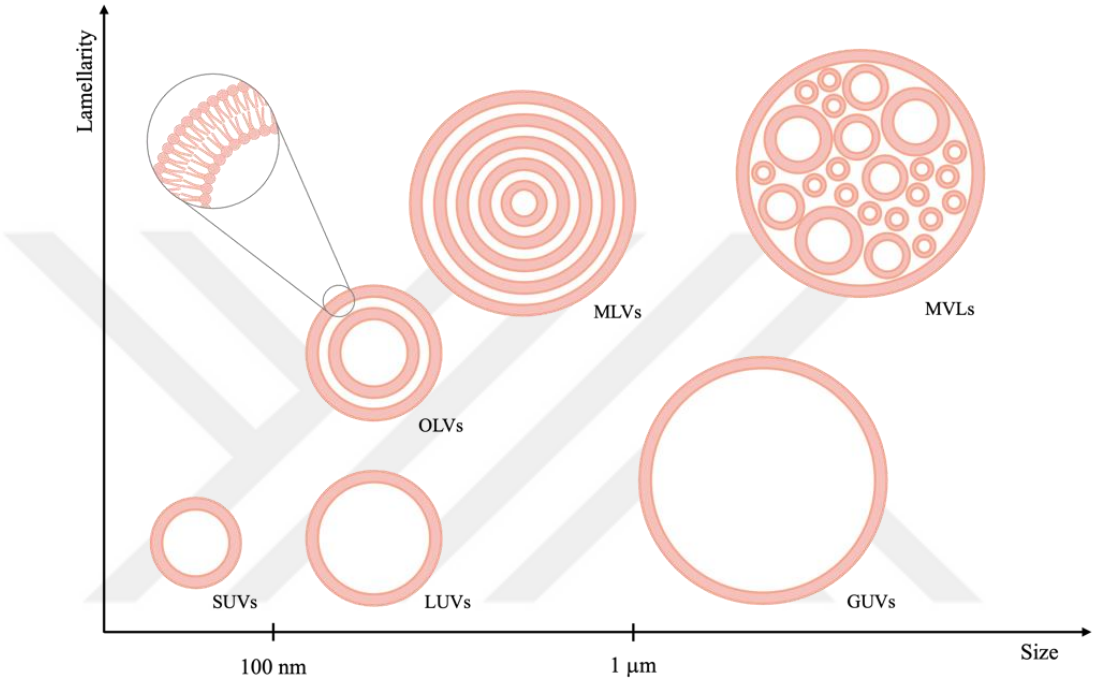

Figure 1. Classification of liposomes according to the number of vesicles. (Modified from Liu et al. (21).)

2.1.1.2 Based on composition

The constitution of liposomes includes three main components phospholipids, cholesterol, and PEG which play roles in formation, stability, and functionality, respectively (22). The main component that makes liposomes is phospholipid which creates spherical vesicles by self-assembly in an aqueous environment due to its amphiphilic nature. The hydrophobic tail and the hydrophilic head structure of the phospholipid bilayer form an amphiphilic structure that gives both hydrophobic and hydrophilic properties. There are basically two types of phospholipids natural and synthetic lipids (23,24). The natural phospholipids have a variety of sources like egg

yolk and soy bean. The classification of phospholipid is basically determined by the polar head group of phospholipid and named phosphatidic acid (PA), phosphatidylcholine (PC), phosphatidylethanolamine (PE), phosphatidylglycerol (PG), and phosphatidylserine (PS), and phosphatidylinositol (PI). Additionally, the fatty acid tail part of natural phospholipids can be composed of saturated fatty acid like palmitic acid, margaric acid, or an unsaturated fatty acid like oleic acid (22–24). Synthetic phospholipids are phospholipids consisting of natural phospholipids with chemically modified polar and non-polar regions (23,25). Stability and the rigidity of liposomes are improved by adding cholesterol to the liposomes' constitution. Cholesterol is a steroid composed of a four-ring structure that incorporates into the phospholipid bilayer of the liposome (22,23,26). Functionally, the surface of liposomes is modified by attaching PEG covalently. PEG is a hydrophilic polymeric steric stabilizer and provides a longer *in vivo* circulation time. Moreover, PEGylated liposomes have an enhanced therapeutic index compared to non-coated liposomes since PEG prevents the recognition by antibodies, and proteolytic enzymes while circulating (22,27). Doxil® is the first PEGylated liposomal formulation approved by the Food and Drug Admisnistration (FDA) in 1995 which contains Dox as an active ingredient and it is introduced to the body intravenously (i.v.) (28). It is used for the management of advanced ovarian, breast cancer, multiple myeloma, and HIV-associated Kaposi's sarcoma. Compared with the free Dox, Doxil® provided greater efficacy and lower cardiotoxicity benefiting from long circulation half-life (45 h) and passive targeting properties due to PEG chains found in its formulation (18). Single-dose vials of 20 mg/10 mL and 50 mg/25 mL are available and administered at a starting rate of 1 mg/min through i.v. infusion to minimize the risk of infusion reactions (29). Dox is an anthracycline anticancer agent with an acid-base dissociation constant (pKa) of 8.3-8.4 and a partition coefficient (log P) of 1.3 (30,31). Moreover, it has anticancer effects through various molecular mechanisms. It causes cancer cell death by accumulating DNA damage by inhibition of Topoisomerase II activity and inhibiting DNA and RNA synthesis by intercalating with DNA and inducing cell cycle arrest (32). It also impairs mitochondrial function by causing the production of ROS and disruption of the mitochondrial membrane potential, leading to apoptosis in cancer cells (33). It has been demonstrated that targeting Dox to tumor mitochondria

eliminates the nuclear effects associated with cardiotoxicity (34). There are also studies that involve colorectal cancer treatments using PEGylated liposomes (6–8,35–37). For instance, oxaliplatin-loaded PEGylated liposomes inhibited the growth of the tumor created in nude mice using SW480 colon cancer cells more than the free oxaliplatin (7).

In general, liposomes are classified as conventional liposomes, stealth liposomes, stimuli-sensitive liposomes, and immuno-liposomes regarding their composition. (Figure 2) (18–20).

The first generation of liposomes are the conventional liposomes which are composed of natural or synthetic phospholipid bilayer either with or without cholesterol (18,23,38). Since the *in vitro* stability of the conventional liposomes was insufficient stealth formulations were invented for enhanced blood circulation (39).

The stealth liposomes also known as long-circulating liposomes include structural modifications by coating with hydrophilic polymer conjugates like PEG (18,20). Wu et al. investigated the effect of different concentrations of cholesterol on the liposomal membrane rigidity where liposomes were composed of soybean phospholipids and PEG. They found out that the concentration of cholesterol in the liposomal formulation affects the diffusivity of the liposome and revealed that moderate cholesterol content provides improved tumor penetration and antitumor effects (40).

The immuno-liposomes also known as ligand-targeted liposomes include ligands like antibodies, peptides, proteins, carbohydrates, and small molecules. This type of surface modification provides *in vivo* site-specific drug delivery (18,20,41). The most commonly used targeting moieties used for immuno-liposomes are immunoglobulins of the IgG class (41). The study done by Lu et al. compared the antitumor activities of free timosaponin AIII (TAIII), TAIII-loaded liposomes, and anti-CD44 antibody-modified TAIII-loaded liposomes. Consequently, they evaluated that antibody-modification was successfully enhanced the antitumor activity of the liposome (42).

The stimuli-sensitive liposomes are chemically activated liposomes by different pH, temperature, or light. The structural state of liposome changes upon intracellular or extracellular stimuli and the release of the drug is promoted (23,43). For instance, the natural phospholipid, 1,2-dioleoyl-sn-glycero-3-phosphoethanolamine (DOPE) has a special bilayer structure that causes membrane destabilization due to pH changes. Soares et al. demonstrated that DOPE-containing liposomes were successfully internalized by endocytosis and increased release of the encapsulated drug into the tumor microenvironment (44).

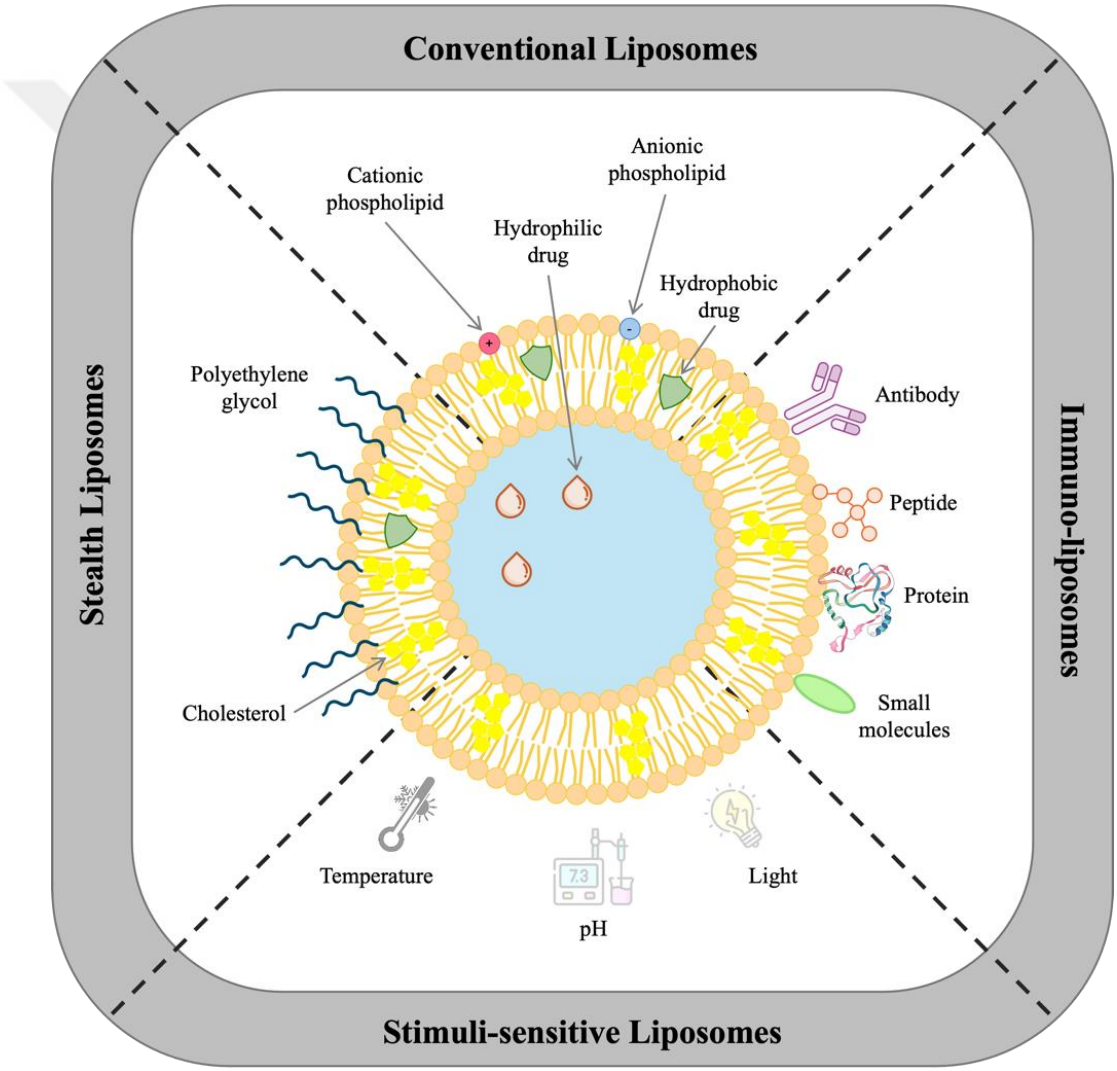

Figure 2. Schematic representation of different types of liposomes. (Modified from Sercombe et al. (18).)

2.1.1.3 Based on methodology

Liposomal formulations can be prepared by varying methods depending on the final characteristics of the liposomes and the drug loading (23). Drug loading methods are divided into two as active and passive drug loading. In passive loading, entrapment of the drug into the liposome is accomplished during liposome preparation. On the other hand, in active loading, the diffusion of the drug through the formulation is driven via buffers or salt solutions (45,46). Each methodology follows four basic steps: evaporation of organic solvent, hydration of lipids in an aqueous media, obtaining final liposomal formulation, and analysis of the final product (19,47). Basically, the methods used for preparing liposomes are divided into two as mechanical dispersion method and the solvent dispersion method. The subcategories of the mechanical dispersion method include thin film hydration (also known as Bangham's method), extrusion, sonication, freeze-thaw, and French pressure cell methods (24,45,47). Although there are various types of liposome preparation the thin film hydration method is the most commonly used method since it creates highly qualified and stable liposomes (24,45,48). In this method, a thin film of lipids is formed by evaporating the organic solvent at a rotary evaporator under reduced pressure followed by hydrating the dried lipid film with aqueous media and extruding through filters to obtain unilamellar vesicles (23,45).

2.1.2 Characterization of liposomes

Liposomes are characterized physiochemically based on their size, PDI, surface charge (or zeta potential), morphology, encapsulation efficiency and *in vitro* release profile (23,49). The size and size distribution of liposomes are determined by dynamic light scattering (DLS) which is a technique that uses the random fluctuations of particles in a solvent known as Brownian motion and measures the intensity of light scattered. This technique is also used for measuring PDI and zeta potential (50,51). For longer circulation time and effective accumulation in the tumor microenvironment the size of liposomal formulations is expected to be lower than 200 nm (52). The PDI of liposomes determines whether liposomal formulation is monodisperse or not.

Formulations with PDI value lower than 0.2 are accepted as monodisperse (53). Another factor that should be taken into consideration during characterization of liposomes is surface charge or zeta potential. Surface characteristics of the liposome is a factor that influences the targeted drug delivery, circulation time, and the cellular uptake capacity. Surface charge can either be cationic, anionic or neutral depending on the formulation (52,54). Formulations with zeta potentials in between or higher than +30 mV and -30 mV are considered as stable (55). The morphological characteristics like shape, internal surface, and size of the liposomes are determined by transmission electron microscopy (TEM). Before TEM analysis, negative staining is applied with uranyl acetate or osmium oxide in order to increase contrast (49,50). The amount of the drug or compound trapped in the liposome is determined by measuring its encapsulation efficiency. Before measuring the encapsulation efficiency, the free drug should be separated from the formulation by ultracentrifugation, dialysis, or gel filtration. After separating the free drug from formulation, the vesicles are disrupted and the released amount of the drug is determined by spectroscopic, enzymatic, or electrochemical techniques (49,56).

2.2 Targeting Mitochondria as a Therapeutic Approach

Targeted drug delivery systems can either be created by the direct conjugation of the drug to the targeting ligand or by linking the targeting ligand to the outer surface of the nanocarrier. Every nanocarrier formulation has its own advantages and limitations (10,11,57).

The mitochondrion has a special bilayer structure which is a promising therapeutic target in the diagnosis and treatment of diseases such as cancer, neurodegenerative diseases, and metabolic diseases. The special structure of a mitochondrion is composed of four parts: the outer mitochondrial membrane (OMM), the inner mitochondrial membrane (IMM), the intermembrane space (IMS), and the matrix. Owing to larger transition pores within the OMM, some of the therapeutic molecules can pass through via passive diffusion. However, since IMM contains smaller transition pores some of the therapeutic molecules cannot arrive through the matrix (58). In addition to this, the

charge distribution between the layers of the mitochondria and also the microenvironment of a cell is responsible for the transport of the therapeutic molecule. The microenvironment of a cell can be considered as two separate parts: outside and inside of the cell. The outer part is positively charged whereas the inner part is negatively charged. The membrane potential of mitochondria (IMM($\Delta\Psi_m$)) and plasma ($\Delta\Psi_p$) is approximately -160-180 mV and -30-60 mV, respectively. Due to the highly negatively charged potential of mitochondria, it becomes harder to send therapeutic molecules to mitochondria. In order to overcome such difficulties, mitochondriotropic moieties were developed which provide direct targeting to mitochondria like TPP, DQA, and mitochondria-targeting peptides (Figure 3) (58,59).

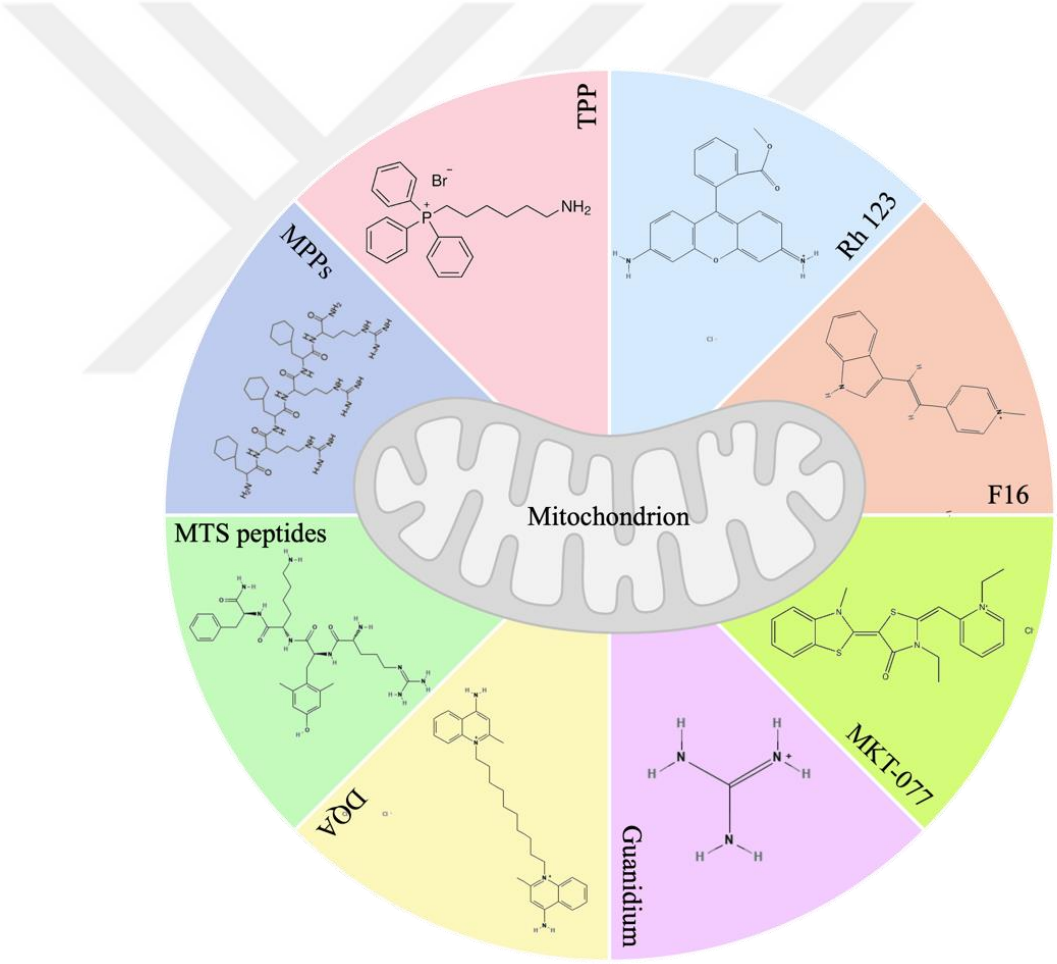

Figure 3. Chemical structures of mitochondriotropic moieties. (Mitochondrion icon: Modified from free icons of BioRender.)

2.2.1 Delocalized lipophilic cations (DLCs)

Delocalized lipophilic cations (DLCs) are positively charged conjugates that make liposomes easily pass through the mitochondrial outer membrane and phospholipid bilayer via diffusion (10). There are six main DLCs used as mitochondriotropic moieties like TPP, Rh 123, F16 ((E)-4-(1H-indol-3-ylvinyl)-N-methylpyridinium iodide), MKT-077, guanidinium, DQA (10,58,60,61). Throughout these DLCs, TPP is the most commonly used mitochondria-targeting ligand (62).

Liposomes which have functionalized surfaces with TPP are successfully targeted through mitochondria and carry their therapeutic cargoes to the mitochondria (Figure 4) (10,11,57). Boddapati et al. created a molecule called stearyl triphenylphosphonium (STPP) which has a conjugated stearyl residue to the TPP in order to make it easier to incorporate into the bilayer of the liposomes. They showed that ceramide-loaded STPP-liposomes had been localized at the mitochondria and found radical decrement in the tumor volume (mouse breast carcinoma 4T1) of BALB/c mice (9). A similar study was done by Patel et al. They found out that the sclareol-encapsulated STPP-liposomes increased the molecule's cytotoxicity and apoptotic effect on the colon cancer cell line, COLO205 (63). However, it has been seen that the toxic effect of empty STPP-liposomes also affected the cytotoxicity of the drug. This situation was overcome by conjugating PEG on the liposomal structure (64). Another study done by Zhou showed that paclitaxel-loaded TPP-PEG-PE liposomes had higher cytotoxic effects on lung cancer (A549) and drug-resistant lung cancer (A549/cDDP) compared to non-targeted paclitaxel-loaded liposomes (1).

There are many studies targeting Dox to mitochondria with different techniques and researchers continue to explore and refine various targeting strategies to optimize efficacy and minimize potential drawbacks (65–71). Chamberlain et al. attached Dox to a mitochondria-penetrating peptide that targets mitochondria and exhibited significant toxicity (65). Cui et al. developed a mitochondria and nucleus dual delivery system that induces elevated levels of apoptosis in Dox-resistant cancer cells (66). Han et al. developed TPP-conjugated Dox and demonstrated that TPP-Dox reverses drug

resistance in MDA-MB-435 cancer cells (67). Hou et al. developed TPP-conjugated chitosan nanoparticles loaded with Dox and demonstrated that Dox-loaded TPP nanoparticles specifically disrupted the mitochondria of tumor cells and improved antitumor efficiency in HeLa and A549 cells (68). Khatun et al. developed Dox-loaded mPEG-TPP conjugates with or without bioreducible disulfide bonds and showed that the bioreducible one can induce fast drug release with enhanced mitochondrial uptake and have a better therapeutic effect than non-bioreducible ones (69). Liu et al. conjugated TPP directly to Dox (TPP-Dox) and linked TPP-Dox to hyaluronic acid (HA-ionic TPP-Dox) to form supra-molecular self-assembled structures to achieve mitochondrial targeting. HA-ionic TPP-Dox significantly inhibited tumor growth and prolonged the survival of tumor-bearing zebrafish compared with free Dox (70). Xiong et al. developed Dox-loaded-hyaluronic acid-modified hydroxyapatite nanoparticles (HAP-HA) that activated the mitochondrial apoptotic cascade and increased in vivo anti-tumor efficacy (71).

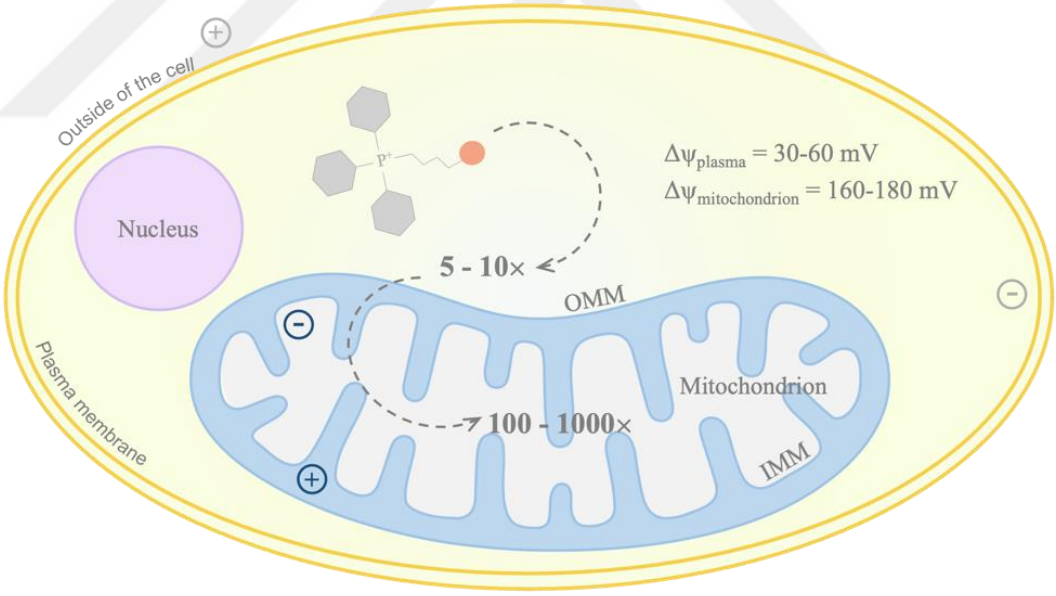

Figure 4. Regulation of cellular uptake of TPP-conjugated compounds through the plasma membrane and mitochondrial membrane potentials (59,61). (Mitochondrion icon: Modified from free icons of BioRender.)

Rh 123 is a cationic dye used as a probe for the localization of mitochondria in living cells (60,72). Biswas et al. conjugated polyethylene glycol

phosphatidylethanolamine (PEG-PE) polymer with Rh 123 to create a mitochondria-targeted paclitaxel-loaded liposomal drug delivery system. They discovered that targeted paclitaxel-loaded liposomes showed enhanced cytotoxicity compared to nontargeted paclitaxel-loaded liposomes or free paclitaxel (73).

F16 ((E)-4-(1H-indol-3-ylvinyl)-N-methylpyridinium iodide) is a novel molecule identified by Fantin et al that exhibits high accumulation in the mitochondrial matrix and disrupts the mitochondrial membrane potential. The disruption of the membrane potential results in the release of cytochrome c, cell cycle arrest, and cell death (60,74). Dubinin et al. created conjugates of betulinic acid with F16 and investigated its mitochondria-targeted effects. They demonstrated that F16-betulinic acid conjugate showed 10-fold higher cytotoxicity than betulinic acid and F16 (75).

MKT-077 (also known as FJ-776) is a rhodacyanine analog that localizes in the mitochondria as the compound enters through the cell (60). MKT-077 itself shows antiproliferative activity against several cancer cell lines including breast cancer, colon cancer, pancreas cancer, and melanomas via its ability to inhibit members of heat shock protein 70 (Hsp70) (76).

Guanidinium is another example of DLC. It is a phototoxic agent that enhances accumulation at the mitochondria due to membrane potential (10). Kang et al. conjugated Gamitrinib with four types of cyclic guanidinium which were monomers, dimers, trimers, and tetramers of cyclic guanidinium. Throughout them, Gamitrinib conjugated with trimers and tetramers showed 6- to 10-fold enhanced anticancer efficacy and higher mitochondrial accumulation compared to monomers and dimers in cancer cells (77).

DQA is also a positively charged lipophilic compound and a topical antimicrobial agent that localizes at the mitochondria of cancer cells and alters the morphology of the mitochondria (60,78). Wang et al. prepared Dox-loaded nanoparticles using DQA as nanoparticle-forming material that selectively targets mitochondria. The results

demonstrated that targeted Dox-loaded nanoparticles showed remarkably higher cytotoxicity than free Dox (79).

2.2.2 Peptide-based targeting compounds

Mitochondria-targeted lipophilic cations can be substituted by mitochondria-penetrating peptides (MPPs) and mitochondria-targeting sequence (MTS) peptides (80,81). MPPs are short synthetic peptides that include both cation and hydrophobic residues in their structure. Thereby, these peptides can penetrate both cellular and mitochondrial membranes independently from the endocytosis pathway which provides an enhanced chance of mitochondrial localization (80,82). Mallick et al. encapsulated antimycin A into a liposome decorated with MPP having a phenylalanine-arginine-phenylalanine-lysine (FRFK) peptide sequence. They evaluated that the cytotoxic effectiveness of the antimycin A was enhanced via the mitochondria-targeting nano-formulation (83). MTS peptides include 20-40 amino acids that provide recognition by receptors at the mitochondrial surface (10,80). Although MTS peptides tend to target mitochondria proteins with high specificity and precision, they exhibit lower efficacy for cellular uptake compared to other mitochondria-targeting compounds due to their poor solubility and large molecular size (80,84). Szeto-Schiller (SS) peptides are small, positively charged mitochondria-targeting peptides that were discovered by Hazel H. Szeto and Peter W. Schiller (85,86). SS peptides selectively target and accumulate in the mitochondria (85,87). For instance, SS-31 is a tetrapeptide composed of D-Arginine-2′6′-dimethylTyrosine-Lysine-Phenylalanine-NH_2 and selectively targets IMM (88).

2.3 Importance of Targeting Mitochondria and Targeted Drug Delivery Systems

Most of the cancer-related deaths occur as a result of metastasis or poor chemotherapy response (89). Conventional chemotherapy is a systemic treatment method that kills the newly dividing cells. Since cancer cells divide more rapidly, treatment kills cancer cells more likely when compared to healthy cells. Since chemotherapy circulates throughout the bloodstream, it may affect other fast-dividing

healthy cells like hair, skin, bone marrow, and the lining of the digestive system. Healthy cells differ from cancer cells metabolically. The disrupted metabolic pathways of cancer cells lead to unregulated cell growth. For cell survival, cells use the oxidation/reduction (redox) reactions which are oxygen-consuming metabolic pathways.

The redox reactions occur at the mitochondrion, the powerhouse of the cell. Mitochondrion is an important organelle for targeting anticancer drugs since it plays key roles in cell proliferation and death. In cancer cells, the altered metabolism refers to the elevated glucose uptake and fermentation of glucose to lactate even in the presence of sufficient oxygen amount. In healthy cells, glucose is converted into pyruvate and it is used for energy production. On the other hand, glucose is converted into lactate in cancer cells. During this conversion of glucose to lactate, lactic acid is produced as a by-product and this production decreases the pH of the cell. This phenomenon is known as aerobic glycolysis or the Warburg effect (90,91).

Although conventional chemotherapy is effective in killing cancer cells, it increases the occurrence rate of metastasis since the treatment is not specific to cancer cells. Metastasis is closely related to the tumor microenvironment (TME) where TME consisting healthy cells, extracellular matrix (ECM), blood vessels, and lymphatics and is a niche for cancer cells (89).

In order to repress the negative effects of chemotherapy, antitumor vehicles are used which improves the efficacy of the treatment simultaneously. For this purpose, nanoparticles are used as drug carriers including liposomes, micelles, and polymers (92). Targeting of nanoparticles to tumor cells could be either active or passive. The working principle of passive targeting depends on the accumulation of the nanoparticle-encapsulated agent at the targeted site. Passive targeting is maintained by the phenomenon called the enhanced permeability and retention (EPR) effect. This phenomenon was first described by Matsumura and Maeda in 1986. The EPR effect occurs as a result of enhanced permeability of the tumor blood vessels and inefficient lymphatic system. Thus, permeability allows nanoparticles to enter through the blood

vessel. Then, since the lymphatic system is dysfunctional, drainage of the nanoparticle from the tumor tissue is prevented and the nanoparticle accumulates within the tumor tissue. Therefore, the EPR effect became the gold standard in anticancer drug design and drug delivery systems since the anatomical nature of tumor blood vessels differs from the normal blood vessels. On the other hand, in active targeting, nanoparticle specifically interacts with the cell via the recognition of specific ligands at the desired (disease) site. Active targeting requires the completion of passive targeting (93,94).

3 MATERIALS AND METHODS

3.1 Synthesis and Characterization of DSPE-PEG-TPP Polymer

To prepare mitochondria-targeted liposomes firstly DSPE-PEG-TPP polymer was synthesized by following the steps shown in Figure 5. For this purpose, 20.6 mg (3-Carboxypropyl) triphenylphosphonium bromide (TPP, #349720, Sigma-Aldrich, USA), 16.6 mg N-Hydroxysuccinamide (NHS, #56480, Sigma-Aldrich, USA), and 27.6 mg N-(3-Dimethylaminopropyl)-N′-ethylcarbodiimide hydrochloride (EDCI, #03450, Sigma-Aldrich, USA) were dissolved in 0.5 mL chloroform ($CDCl_3$, #1.02445.2500, Merck, Germany) and stirred at room temperature for 2 h under dark conditions. At the end of 2 h, 100 mg DSPE-PEG_{2000}-NH_2 (#880128C, Avanti-Polar Lipids, USA) and 2.5 μL triethylamine (TEA, #T0886, Sigma-Aldrich, USA) were added to the mixture and then stirred at room temperature (RT) for 24 h under nitrogen. Then $CDCl_3$ was evaporated using a rotary evaporator (Stuart, #RE300, Keison Products, UK), and the crude product was dissolved in 2 mL of double distilled water (ddH_2O). A turbid solution was obtained as soon as the crude product was dissolved. All of the solution was introduced into the dialysis membrane (MWCO: 2 kDA, 18 mm flat width #132620, SpectrumLabs, USA) and dialysis was started against distilled 1L distilled water for 24 h. Then, the dialysate was freeze-dried using lyophilization (FreeZone 6 Plus, #7934020, Labconco, USA) and the purity of the DSPE-PEG-TPP polymer was characterized by proton nuclear magnetic resonance (^{1}H-NMR, Bruker 400MHz NMR) at Boğaziçi University (64). The pure DSPE-PEG-TPP polymer was stored as powder at 4 °C for future studies.

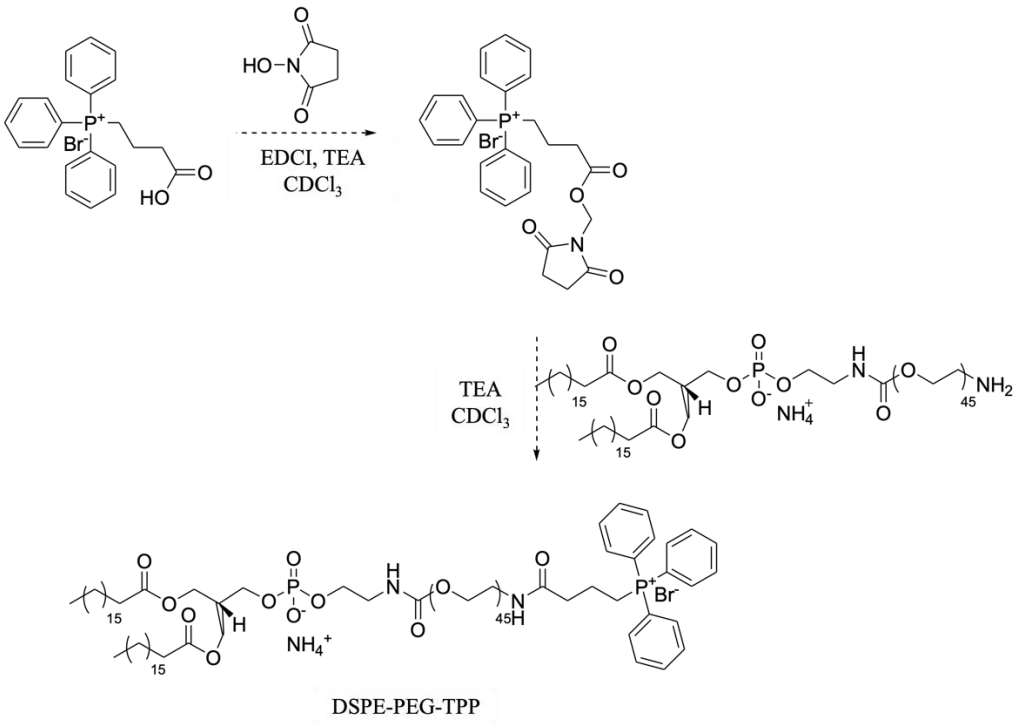

Figure 5. Steps of DSPE-PEG-TPP polymer synthesis.

3.2 Preparation of Liposomes

According to their formulations, six different liposomes were prepared and each had a different function:

a. Empty PEG-PE liposomes (PPL)
b. Empty TPP-PEG-PE liposomes (TPPL)
c. Rhodamine B-labeled PEG-PE liposomes (RhB-PPL)
d. Rhodamine B-labeled TPP-PEG-PE liposomes (RhB-TPPL)
e. Doxorubicin-loaded PEG-PE liposomes (Dox-loaded PPL)
f. Doxorubicin-loaded TPP-PEG-PE liposomes (Dox-loaded TPPL)

Each liposome was prepared separately using Bangham's thin film hydration method (Figure 6) which includes five fundamental stages: lipids dissolution in organic solvent, evaporation of organic solvent (thin lipid film formation), hydration of dried lipid, self-assembly of the liposomal vesicles, and characterization (1,64,95).

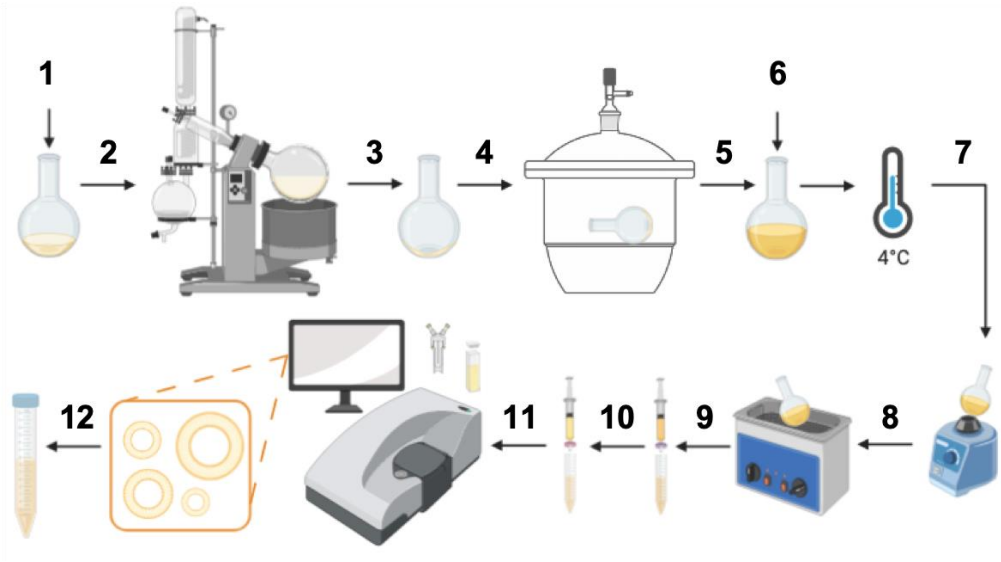

Figure 6. Steps of thin film hydration method. (Modified from free icons of BioRender.)

The steps shown in Figure 6 can be listed as (1) Dissolving materials in dehydrated DCM and introduce into round bottom flask. (2) Evaporation of organic solvent (DCM) using rotary evaporator. (3) Thin film formation. (4) Overnight incubation of the thin lipid film for the removal of excess organic solvent under vacuum desiccator. (5-6) Hydration of the thin lipid film with 1X DPBS (pH 7.4) and overnight incubation at 4 °C. (7) Separation of the hydrated thin lipid film from the round bottom balloon by vortexing the hydrated film with glass beads. (8) Sonication of the formulation for 30 min in an ultrasonic bath. (9) Filtration through 0.45 µm syringe filter for once. (10) Filtration through 0.22 µm syringe filter for twice. (11) Characterization of the obtained liposomes using dynamic light scattering method. (12) Keeping the formulation at 4 °C for short term storage.

3.2.1 Preparation of empty TPPL and PPL

Dichloromethane (DCM, #106050, Merck, Germany) was used for preparing liposomal thin films as an organic solvent. Before using DCM, 10 mL of DCM was dried with 2 g anhydrous sodium sulfate (Na_2SO_4, #1.06649.1000, Merck, Germany) by mixing them on a magnetic stirrer at RT for an hour. Then, the dried DCM was filtered and kept under an atmosphere of dry nitrogen. Empty TPPL and PPL were

prepared by mixing cholesterol: L-α-PC: DSPE-PEG-TPP or PEG-PE in the ratio of 1: 0.92: 0.08 (mole %). Briefly, all ingredients were dissolved in dried DCM according to the liposomal formulation, and then lipid film was formed in a rotary evaporator. The excess amount of DCM was removed using a vacuum desiccator overnight. Then, the dried thin lipid film was hydrated with 4 mL of 1X DPBS, pH 7.4 (#14190094, ThermoFisher Scientific, USA), and allowed for self-assembly overnight at 4 °C. The hydrated product was sonicated for 30 min in an ultrasonic bath (#621.05.003, Isolab, Germany). Then, the final liposomal formulation was obtained by filtering once through sterile 0.45 μm (Membrane: PES, 33 mm, #99745, TPP, Switzerland) and twice through sterile 0.22 μm syringe filters (Membrane: PES, 33 mm, #99722, TPP, Switzerland).

3.2.2 Preparation of RhB-TPP-PEG-PE and RhB-PEG-PE liposomes

To monitor empty TPPL and PPL *in vitro* environments, RhB-TPPL and RhB-PPL were prepared using the thin film hydration method by adding the fluorescent tracking dye 0.005 mole % of Lissamine™ Rhodamine B 1,2-Dihexadecanoyl-sn-Glycero-3 Phosphoethanolamine, Triethylammonium Salt (Rhodamine DHPE, RhB, #L1392, ThermoFisher Scientific, USA) to the composition of the liposomes containing cholesterol: L-α-PC: DSPE-PEG-TPP or PEG-PE in the ratio of 1: 0.92: 0.08 (mole %) (96).

3.2.3 Preparation of Dox-loaded TPPL and PPL

To prepare Dox-loaded TPPL and PPL, Dox (#sc-200923A, Santa Cruz Biotechnology, USA) stock solution in methanol (10 mM) (#1.06008.2500, Merck, Germany) was added to the lipid mixture with a final concentration of 100 μM in DCM, and liposomes were prepared by the thin film hydration method as described above (1,64,95). To separate free (non-incorporated) Dox from the Dox-loaded TPPL and PPL, the formulations were ultracentrifuged (OptimaTM, MAX-TL Ultracentrifuge, Beckman Coulter, USA) at 200,000 xg, 4 °C for 16 h. After ultracentrifugation, the supernatant was discarded (which includes non-

incorporated/free Dox) and then the pellet was washed with 1 mL of sterile ddH_2O twice. After separating the free Dox, Dox-loaded TPPL and PPL were characterized and the concentration of the Dox encapsulated into the liposomes was determined according to calibration curve created with Dox standard solutions dissolved in 1X DPBS mixed with 100 % ethanol (#1.00983.2500, Merck, Germany) at 1: 1 ratio.

3.3 Characterization of Liposomes

The particle size, PDI, zeta potential (surface charge), and stability of liposomes were measured using the DLS technique (LiteSizer 500; Anton-Paar).

3.3.1 Size distribution

The size distribution of liposomes was determined by the mean hydrodynamic diameter using LiteSizer 500 (Anton Paar, Austria) which uses DLS as a measurement technique. The average size of particles was represented as mean ± standard deviation (STD) (n=3).

3.3.2 Surface charge

The surface charge of the liposomes was determined by the zeta potential using LiteSizer 500 (Anton Paar, Austria) which DLS as a measurement technique. For zeta potential measurements the liposomes were diluted (sample: diluent, 1: 10) in 1 mM sodium chloride (NaCl, #13423, Sigma-Aldrich, USA) in a clean eppendorf tube and then introduced into omega cuvettes (#225288, Anton Paar, Austria) for measurement.

3.3.3 Morphology

The morphology of the liposomes was determined by using a transmission electron microscope (TEM, Talos L120C, ThermoFisher Scientific, USA). For TEM analysis, 10 μL of liposomes was introduced onto the copper grids (#TEM-

LC200CU100, Sigma-Aldrich, USA) and then negative staining was done with 2 % uranyl acetate (#22400, Electron Microscopy Sciences, USA).

3.3.4 Stability of liposomes

To investigate the stability of the liposomes, their mean particle size (hydrodynamic diameter), zeta potential (charge distribution), and PDI of the empty TPPL and PPL were incubated at 4 °C, RT, and 37 °C for 8 weeks. The changes in the liposomes' size and charge distribution were recorded every month at 4 °C, RT, and 37 °C.

3.3.5 Encapsulation Efficiency of Dox-loaded TPPL and PPL

The final concentration of the encapsulated Dox in Dox-loaded TPPL and PPL was determined by using a spectral scanning multimode reader (VarioSkan Flash, Thermo Scientific, USA). For this purpose, a calibration curve special to Dox (0.625-40 μM) was created and the fluorescence intensity of the solution was measured at the spectrum of excitation/emission 470/490-800 nm where the maximum fluorescence intensity was observed at 590 nm (λ_{max}). Then, the final concentration of the encapsulated Dox was calculated according to the equation of a linear line. Both empty TPPL and PPL (used as blank) and Dox-loaded TPPL and PPL were distorted with 100 % ethanol for complete release of Dox from the liposomal vesicle. Then, the encapsulation efficiency of Dox was determined by the following equation: encapsulation efficiency (%) = (C_f / C_i) × 100 where C_f is the final concentration of Dox calculated and C_i is the initial concentration of Dox added into the liposomal formulation (97).

3.4 Determination of *In Vitro* Drug Release Profile

The Dox release profiles were determined using the dialysis method (98). Briefly, Dox-loaded TPPL and PPL were added to a dialysis tubing (MWCO: 10 kDa, 32 mm flat width, #HR10-32-5, CelluSep, USA) and then introduced into a tube either filled

with PBS pH 7.4 (#P4417, Sigma-Aldrich, USA) with 0.01 % Tween-80 (#9005-65-6, Research Products International, USA) or 0.1 M acetate buffer pH 5.6 with 0.01 % Tween-80 with a ratio of 1: 80 (liposome: buffer). The tubes were incubated at 37 °C with a constant stirring speed of 100 rpm. A sample from the receptor solution was collected at predetermined time points (0.25, 0.5, 0.75, 1, 2, 3, 4, 5, 24, 48, 72, and 96 h) and the collected volume was replaced with the same amount of fresh buffers. The Dox content released into the receptor buffer was determined by a spectral scanning multimode reader (VarioSkan Flash, Thermo Scientific, USA) and using the calibration curve constructed where the fluorescence intensity of the standard solutions was measured at the spectrum of excitation/emission 470/490-800 nm. The maximum fluorescence intensity was observed at 595 nm (λ_{max}). Then, the released amount of Dox was calculated from the calibration curve constructed in both pH 7.4 and pH 5.6 buffer with 0.01 % Tween-80.

3.5 Maintenance of Cell Culture

HCT116, human colorectal carcinoma 116 cell line was a kind gift from Dr. Thomas Kunkel (National Institutes of Health (NIH) / National Institute of Environmental Health Sciences (NIEHS), USA). The growth medium of the cells was Dulbecco's modified eagle medium (DMEM, #31330-038, Gibco, USA) containing 10 % Fetal Bovine Serum (FBS, #10270106, Gibco, USA), and 1 % Penicillin/Streptomycin (Pen/Strep, (#15140122, LifeTech, USA). The culture was maintained at 37 °C incubator with humidified atmosphere of 5 % CO_2 (ThermoFisher Scientific, USA).

3.6 Cellular and Mitochondrial Uptake of Liposomes

The quantification of the cellular uptake of free Dox, Dox-loaded TPPL, and Dox-loaded PPL was performed by flow cytometry analysis (1,64). The day before analysis, 300.000 cells/well were seeded in 6-well plates. Then, cells were incubated in the presence of 5 μM of free Dox, and Dox-loaded liposomes for 1 h at 37 °C and 5 % CO_2 incubator. At the end of 1 h incubation, cells were washed with 1X DPBS, pH 7.4

twice in order to get rid of dead/detached cells. Then, cells were collected by trypsinization. Then, the collected cells were centrifuged at 600 xg for 5 min, and then washed with ice-cold 1X DPBS, pH 7.4 twice before analysis. Then, the quantification of the uptake of liposomes into the cell was performed via flow cytometry on the PE-A channel. The data were analyzed by BD FACSuite software (1,64). HCT116 cells that were not incubated with liposomes were used as a control.

The mitochondrial co-localization of RhB-TPPL, RhB-PPL, Dox-loaded TPPL, and Dox-loaded PPL in the mitochondria and the cell was visualized with a confocal microscope (#LSM700, Carl Zeiss, Germany) using the MitoTracker Green FM dye (MTG, #M7514, ThermoFisher Scientific, USA) after incubating with HCT116 cells at 37 °C and 5 % CO_2 incubator for 4, 8, and 24 h with the liposomes. The red color of RhB and Dox with the green color of MitoTracker Green was displayed as yellow-orange for liposomes localized in mitochondria. The nucleus was visualized by using SlowFade diamond antifade mountant with DAPI (#S36968, ThermoFisher Scientific, USA) as a fluorescent dye. To detect the fluorescence of RhB, MTG, and DAPI, lasers at 560, 488, and 405 nm were used, respectively (64,99).

3.7 *In vitro* Cytotoxicity of Empty and Dox-loaded Liposomes

For the cytotoxicity of empty TPPL and PPL, impedance-based real-time detection of cell proliferation and cytotoxicity experiments were performed according to the instruction manual of the xCELLigence Real-Time Cell Analysis (RTCA) DP (dual purpose) instrument (Acea Biosciences, USA). Approximately 22 h after seeding 12.000 cells/well in E-plate 16, when the cells were in the log growth phase the cells were treated with increasing concentrations of empty TPPL and PPL and monitored every 30 min for 96 h. The cells were also treated with a final concentration of 0.01 % PBS which served as a vehicle control. The results were expressed by normalized cell index (CI), which was derived from the ratio of CIs before and after the addition of molecules (100).

The cytotoxic effects of free Dox and Dox-loaded TPPL and Dox-loaded PPL were measured in HCT116 cells using WST-8 assay (CCK-8 assay, #AB228554, Abcam, UK) according to the manufacturer's instructions. Briefly, 5×10^3 HCT116 cells per well were seeded in 96-well plates and incubated overnight at 37 °C, 5 % CO_2 incubator. Then, the cells were treated with different concentrations of free Dox, empty TPPL and PPL, Dox-loaded TPPL, and Dox-loaded PPL and incubated for 48 h at 37 °C, 5 % CO_2 incubator. Subsequently, WST-8 reagent was added into each well and the absorbance of each well was measured at 460 nm using a plate reader (Powerwave XS2, BioTek, Vermont, USA). The percent cell survival was calculated as the mean values (OD 460 nm) of three independent experiments performed in triplicates to that of corresponding control cells multiplied by 100. The control cells for the normalization were the untreated, empty TPPL, and empty PPL cells. The IC_{50} values were calculated using GraphPad Prism 9.3.1 software.

3.8 Reactive Oxygen Species (ROS) Measurements

A cellular ROS indicator 2',7'-dichlorodihydrofluorescein diacetate (H_2DCFDA, #D399, ThermoFisher Scientific, USA) was used to measure cellular ROS according to the manufacturer's instructions. Briefly, 2×10^4 HCT116 cells per well were plated in clear bottom black-walled 96-well plates. Following overnight incubation at 37 °C, 5 % CO_2 incubator, the cells were treated with 5 μM free Dox, Dox-loaded TPPL, and Dox-loaded PPL alone or in combination with the ROS scavenger 1 mg/mL N-Acetyl cysteine (NAC, #A9165, Sigma-Aldrich, USA) for 24 h. Then, the cells were incubated with 10 μM H_2DCFDA for 45 min at 37 °C, 5 % CO_2 incubator. ROS levels were measured at ex/em 485/535 nm using a multimode microplate reader (VarioSkan Flash, ThermoFisher Scientific, USA). The experiment was repeated three times. Fluorescence data were normalized to the corresponding cell viability data, which was measured using the WST-8 assay according to the manufacturer's instructions (100).

3.9 Statistical Analysis

All quantitative data were presented as the mean ± STD of three experiments. Statistical analysis was performed using a two-tailed Student's t-test for pairwise comparison and one-way ANOVA with multiple comparisons by Tukey post-hoc tests for multiple comparisons. Statistical analysis was performed using the GraphPad Prism 9.2.0 software. $p < 0.05$ was considered statistically significant.

4 RESULTS

4.1 Synthesis and Characterization of DSPE-PEG-TPP Polymer

TPP was conjugated to DSPE-PEG which is a very useful material for the formulation of liposomes for achieving prolonged blood circulation time, improved stability, and enhanced encapsulation efficiency (101). Figure 7 shows that the TPP-conjugated amphiphilic DSPE-PEG polymer has been successfully synthesized and obtained in pure form. The proton NMR analysis was conducted in $CDCl_3$ as the solvent, with a peak of 7.24 ppm. The reference peak seen at 0 ppm is the tetramethyl silane (TMS) signal, which is the internal standard substance in the solvent. The multiplet seen in the spectrum around 7.2-7.4 ppm comes from the aromatic protons of the TPP molecule. The peak around 8 ppm belongs to the amide proton in the molecule and since this proton is labile the integral value was not consistent which is an expected situation in $CDCl_3$. The $–OCH_2$ protons in the ethylene glycol monomers of the DSPE-PEG chain appeared as a broad peak around 3.6 ppm, as expected. The aliphatic CH_2 protons of polyethylene (PE) chains appeared at 1.23 ppm. The two ester protons ($–C{=}OOC\mathit{H}_2$) at the end of the DSPE-PEG chain and the four ester protons in the PE chains appear in the 4.4-3.8 ppm range. Based on their integration ratio, it can be understood that the reaction occurred at a one-to-one ratio of TPP molecule and DSPE-PEG polymer. The integration of DSPE-PEG ester protons, especially their retention with the tertiary 1 proton in the PE polymer indicates that the polymer preserves it chemical structural integrity. Moreover, the integration of this tertiary proton peak, as the value of 1, is consistent with the aromatic 15 protons of the TPP molecule, proving that there is no TPP-derived impurity left in the product.

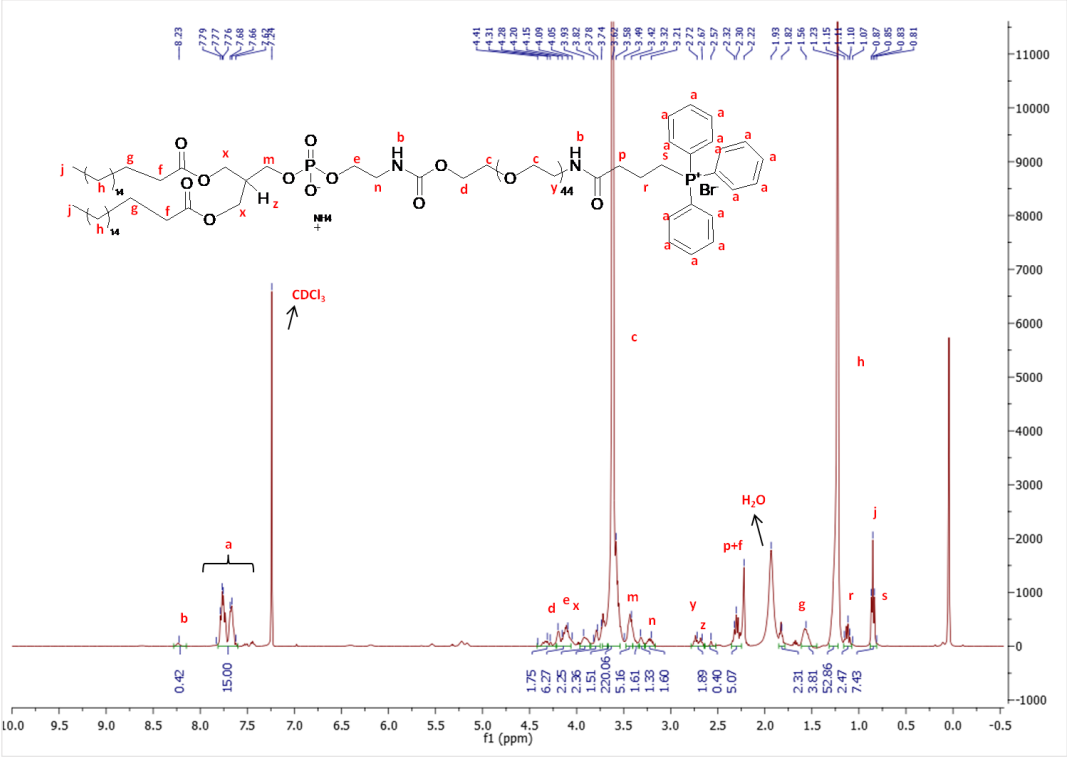

Figure 7. NMR spectrum of DSPE-PEG-TPP polymer.

4.2 Characterization of Empty and Dox-loaded Liposomes

The characterization results of liposomes are presented in Table 1. The zeta potential measurement demonstrates that the surface charge of the PPL, Dox-PPL, and RhB-PPL is negative due to PEG-PE, and that of TPPL, Dox-TPPL, and RhB-TPPL is positive due to TPP. The values given in Table 1 show the mean ± STD of three independent experiments. The size of all liposomal formulations is lower than 200 nm.

Table 1. Physicochemical properties of liposomes.

Formulation	Particle Size (nm)	Polydispersity index (PDI)	Zeta potential (mV)
Empty PPL	117.51 ± 2.82	0.19 ± 0.02	-13.20 ± 0.30
Empty TPPL	135.76 ± 4.29	0.15 ± 0.01	6.07 ± 0.17
Dox-PPL	109.66 ± 2.09	0.20 ± 0.01	-23.63 ± 0.21
Dox-TPPL	126.50 ± 1.29	0.18 ± 0.02	9.97 ± 0.90
RhB-PPL	147.89 ± 1.31	0.15 ± 0.03	-14.97 ± 0.31
RhB-TPPL	157.65 ± 0.18	0.18 ± 0.03	6.80 ± 0.00

Data are presented as mean ± STD (n=3).

The amount of the encapsulated drug in the liposomes was determined by using a spectral scanning multimode reader (VarioSkan Flash Plate Reader, Thermo Scientific). The fluorescence intensity of the formulation was measured at 590 nm (λ_{max}) which was the wavelength that Dox gave the maximum fluorescence intensity after the distortion of liposomal vesicles using 100 % ethanol. Then by using the calibration curve specific to Dox, the concentration of the drug encapsulated in the liposomal formulation was calculated (Figure 8). Dox-loaded liposomes showed similar characteristics to empty liposomes through both size and charge distribution (Table 1). According to the calculations, the encapsulation efficiency of Dox in PPL, and TPPL were found to be 23.79 %, and 11.13 %, respectively. Although encapsulation efficiency was low, it was sufficient for *in vitro* analysis in this study.

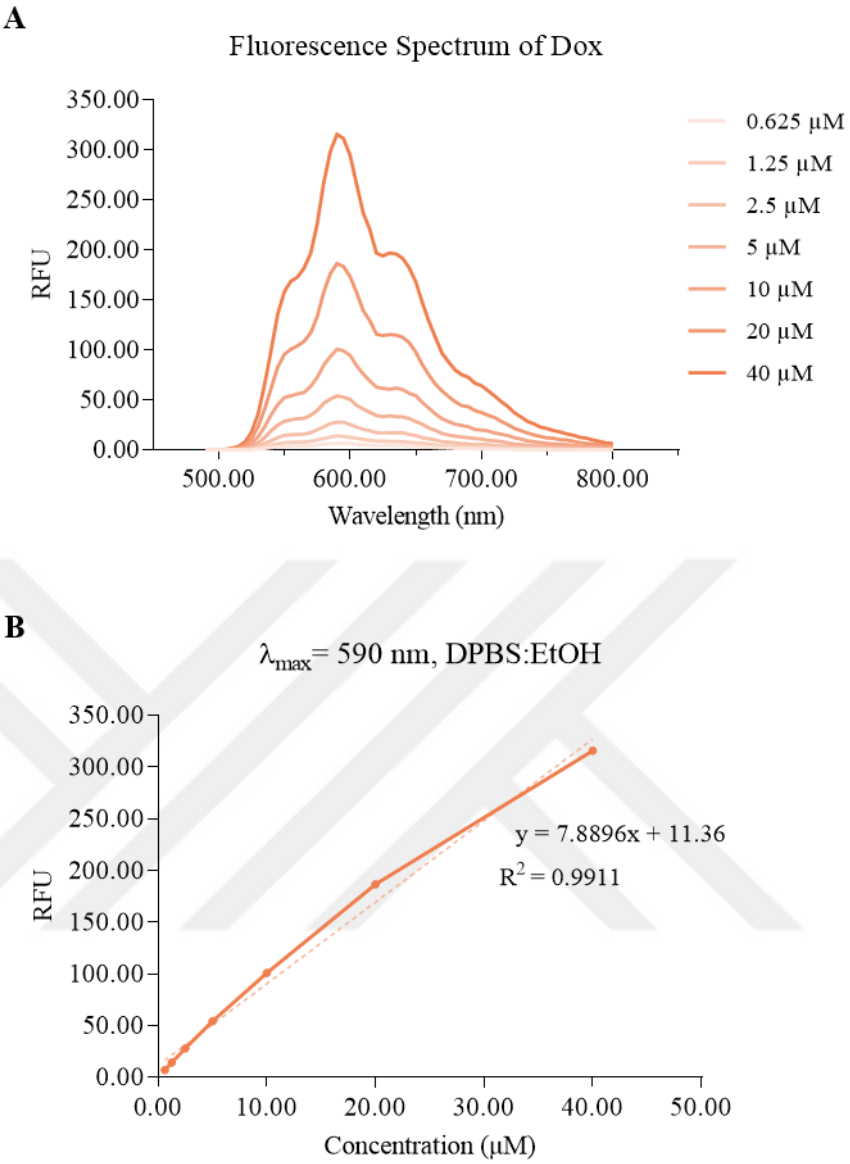

Figure 8. Spectrophotometric analysis of Dox. A. Fluorescence spectra of various concentrations of Dox. B. Calibration curve for Dox solution in DPBS: EtOH.

TEM images of empty and Dox-loaded TPPL and Dox-loaded PPL are presented in Figure 9. TEM results demonstrate that the liposomes were structurally spherical, the core parts of Dox-loaded ones were dark black (filled) (Figure 9B, 9D), and the core parts of empty liposomes were light gray (empty) (Figure 9A, 9C). Since TEM images were taken under a high vacuum, water in the aqueous core of the liposomes may evaporate, and thus liposomes may shrink as the water evaporates.

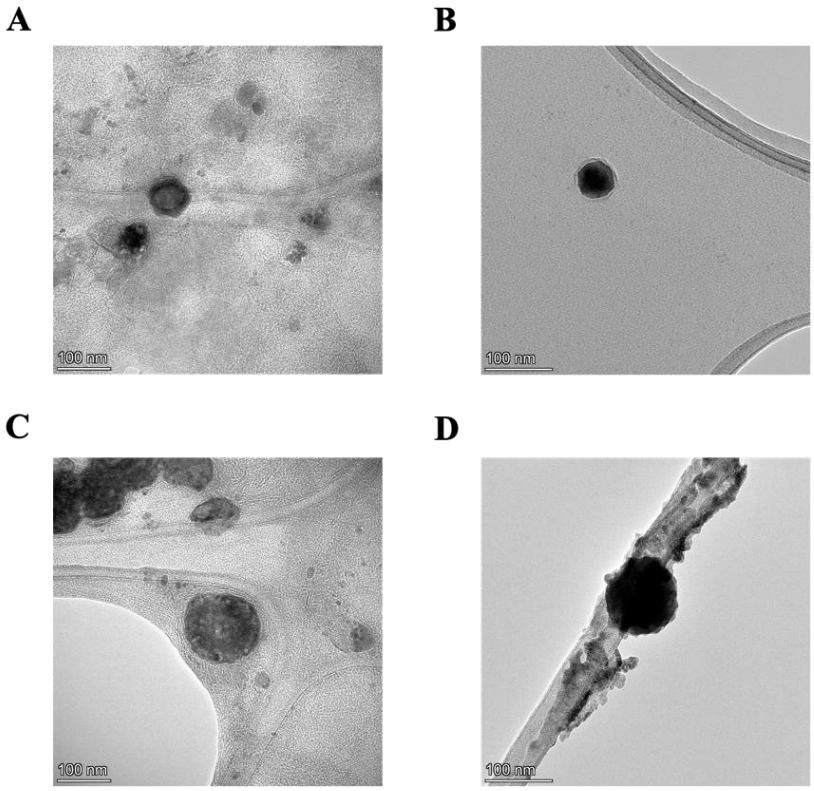

Figure 9. TEM images of PEG-PE and TPP-PEG-PE liposomes. A. Empty PPL (100 nm). B. Dox-loaded PPL (100 nm). C. Empty TPPL (100 nm). D. Dox-loaded TPPL (100 nm).

4.3 Stability of Empty TPPL and PPL

The stability of the liposomal formulations depends on both chemical factors such as oxidation of the lipid content and the formation of free radicals in fatty acid tails and physical factors, such as storage temperature and environment (102). For the stability analysis of empty TPPL and PPL, the time- and temperature-dependent changes (4 °C, RT, and 37 °C) in their sizes, PDI values, and zeta potentials were measured weekly and followed for 8 weeks (Figure 10). No statistically significant changes were observed in the size of TPPL and PPL over 8 weeks at 4 °C and RT (Figures 10A and 10B). There were no significant changes in the size of PPL for 8 weeks at 37 °C whereas fluctuations were observed in the size of TPPL (Figure 10C). The PDI value of PPL did not change statistically significantly at all temperatures for 8 weeks but it was more stable at 4 °C (Figure 10D). The PDI value of TPPL did not

change significantly and was around 0.2 at 4 °C and RT for 8 weeks but increasing RT to 37 °C caused an increment in the PDI values of TPPL (Figure 10E). The zeta potentials for PPL were negative at all temperatures for 8 weeks (Figure 10F) whereas TPPL lost its positive surface charge and became negative after a month at 37 °C (from 5.77 ± 0.15 to -5.00 ± 0.10) (Figure 10F). The zeta potentials for TPPL were positive at RT for 8 weeks but decreased from 6.07 ± 0.32 to 2.00 ± 0.17 after a month (Figure 10F). It can be concluded that considering all parameters, both PPL and TPPL are more stable at 4 °C (Figure 10).

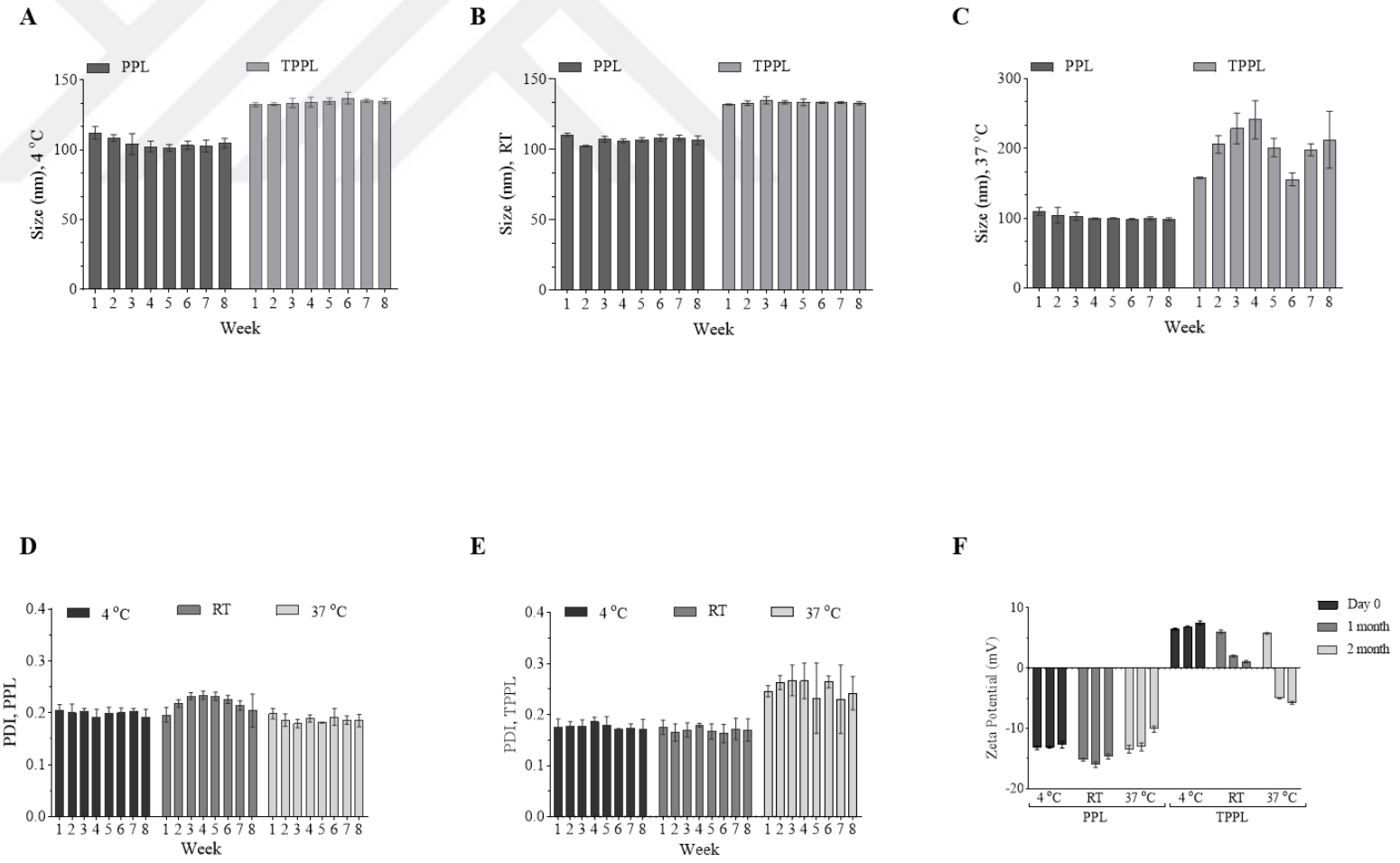

Figure 10. Stability of empty liposomes. Time- and temperature-dependent changes according to A-C. size, D-E. PDI, F. Zeta potential.

4.4 Cellular Uptake and Cytotoxicity of Empty TPPL and PPL

To track empty TPPL and PPL *in vitro* environments, RhB-TPPL and RhB-PPL were prepared and characterized (Table 1). The localization of RhB-TPPL in the mitochondria was visualized by a confocal microscope using MitoTracker Green for staining mitochondria after incubating with HCT116 cells for 4, 8, and 24 h with RhB-labeled liposomes. The red color of RhB and the green color of MitoTracker Green are displayed as yellow/light orange for liposomes localized in mitochondria. The nucleus was stained with DAPI (64,99). Figure 11A shows that RhB-PPL, which has no mitochondria targeting group, did not localize to mitochondria at all the time points tested (Figure 11B, merged green dots). In Figure 11B, RhB-TPPL with the mitochondria targeting group DSPE-PEG-TPP started to localize in the mitochondria from the 4^{th} h and its localization increased at the 8^{th} and then 24^{th} h (Figure 11B, merged, yellow/light orange dots).

The effect of empty TPPL and PPL on the viability of HCT116 cells was determined by the xCELLigence RTCA DP system. TPPL and PPL were applied to the cells at five different concentrations and did not show any cytotoxic effect on the cells even at the highest concentration applied (Figure 11C).

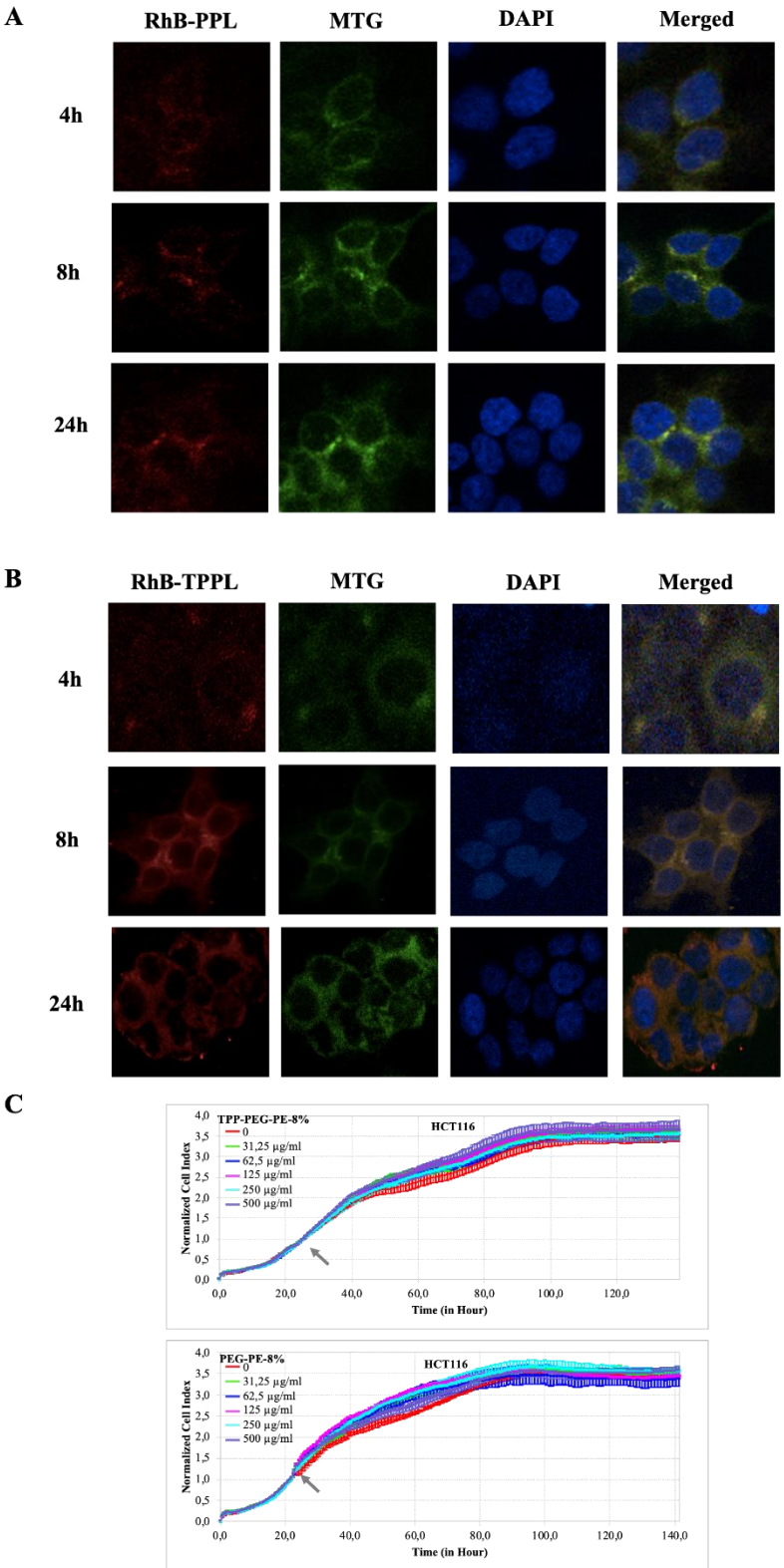

Figure 11. Cellular uptake of RhB-PPL and RhB-TPPL in HCT116 cells. A. Confocal microscopy images of RhB-PPL. B. Confocal microscopy images of RhB-TPPL. C. Cytotoxic effect of empty TPPL and PPL on cellular proliferation of HCT116 cells. Grey arrow: Application time of different concentrations of empty liposomes.

4.5 Cellular Uptake of Dox-loaded Liposomes

The cellular uptake capacity of Dox-loaded TPPL and PPL was quantified by flow cytometry analysis (103). When the population of unstained cells and treated cells were compared, shift was observed indicating that Dox-loaded liposomes were internalized within the cells. According to the fluorescence intensities obtained, Dox uptakes from PPL and TPPL were increased by 1.36 ± 0.05-fold, and 1.51 ± 0.14-fold compared to free Dox upon 1 h of incubation, respectively (Figure 12A).

Intracellular delivery of Dox-loaded TPPL and PPL was also confirmed via confocal microscopy imaging. The overlap of the red color of Dox and the green color of MitoTracker Green is displayed as yellow/light orange for liposomes localized in mitochondria. The nucleus was stained with DAPI. Dox-loaded TPPL was localized in the mitochondria starting from the first time-point (4^{th} h) (Figure 12B) whereas Dox-loaded PPL did not localize in mitochondria (Figure 12C). The intensity of localization of Dox-loaded TPPL was increased as incubation time increased from the 8^{th} to the 24^{th} h. (Figure 12C). Thus, Dox-loaded TPPL was accumulated in mitochondria in a time dependent manner.

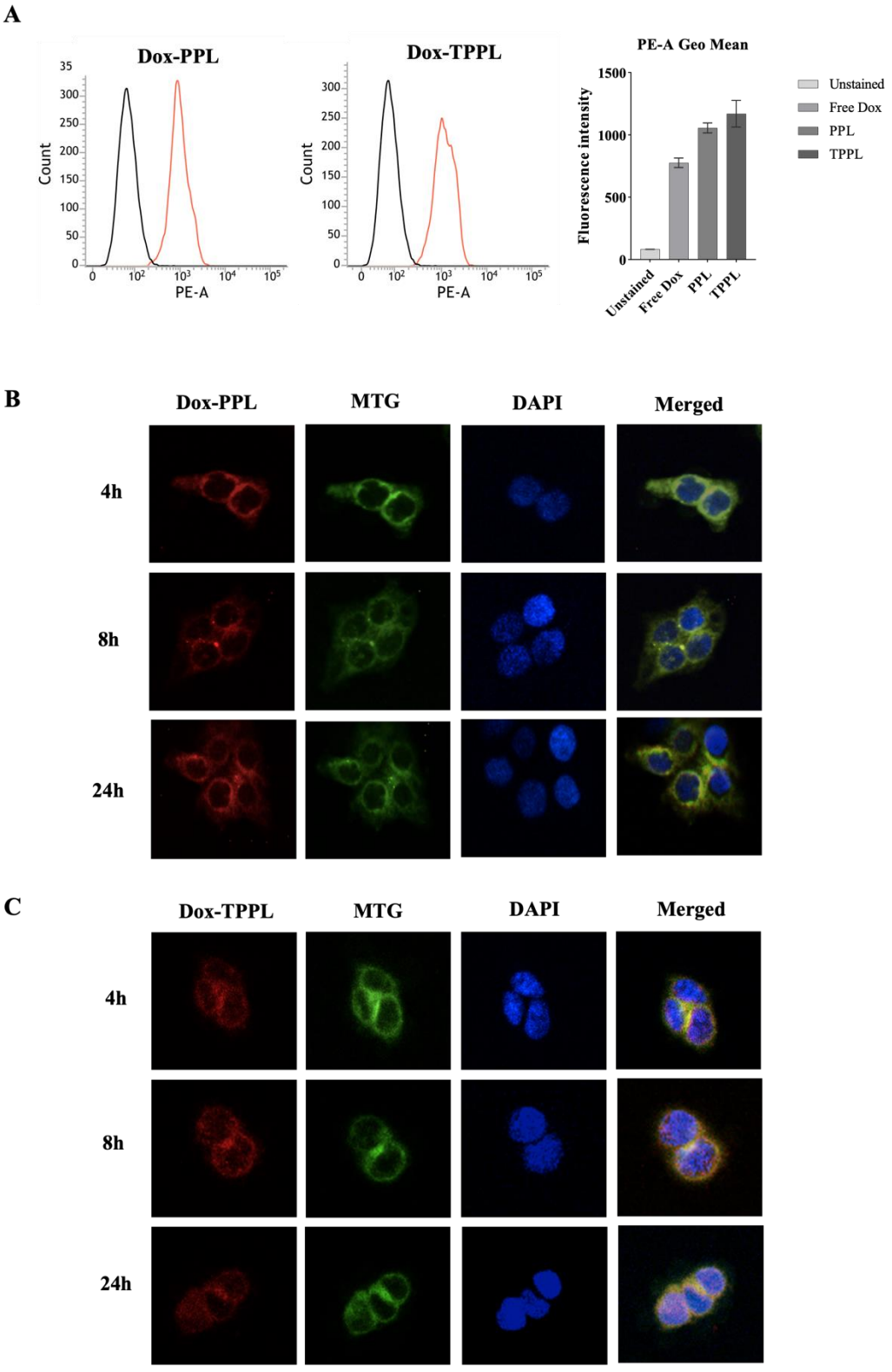

Figure 12. Cellular uptake of Dox-loaded PPL and TPPL in HCT116 cells. A. Flow cytometry data of HCT116 cells incubated with Dox-loaded liposomes. B. Confocal microscopy images of Dox-loaded PPL. C. Confocal microscopy images of Dox-loaded TPPL.

4.6 Drug Release Profile

Different concentrations of Dox, ranging from 0.02 to 2 μM were used for the construction of the calibration curve and plotted the mean absorbance value versus the concentration of Dox (Figure 13). Since the pH of the tumor tissue is acidic (pH 5.6-6.8) (3,70). the *in vitro* release profile of Dox-loaded PPL and TPPL were analyzed at two different pH; physiological pH 7.4 and acidic pH 5.6 at 37 °C (Figure 14). The Dox calibration curve was recorded at the wavelength of 595 nm (λ_{max}). The linear range of the calibration curve obtained for the Dox solution showed good linearity and the R square of the regression equations were 0.9998 and 0.9999 for pH 7.4 and pH 5.6, respectively (Figure 13).

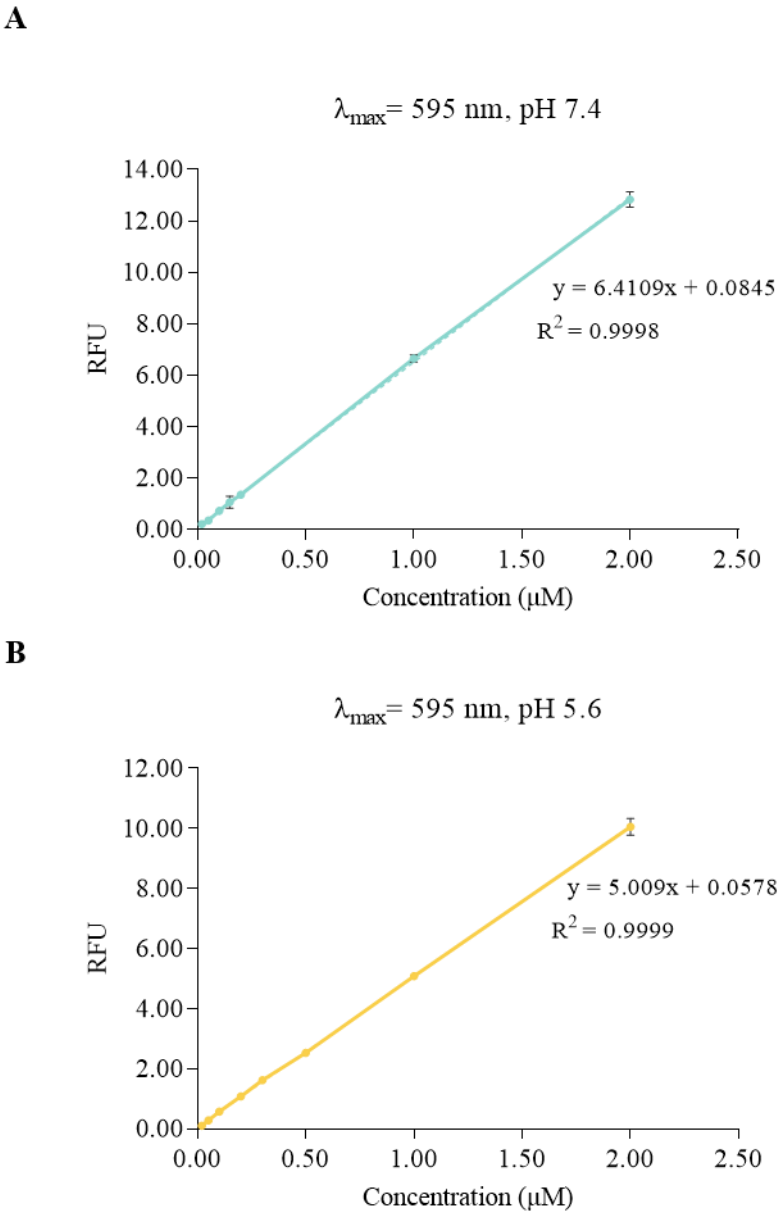

Figure 13. The calibration curve for the Dox solution at A. pH 7.4 and B. pH 5.6.

The amount of Dox released from TPPL increased statistically significantly at pH 5.6 compared to pH 7.4 (Figure 14A). In 1 h incubation, 10.09 ± 1.08 % of Dox was released from TPPL at pH 7.4 whereas 20.23 ± 1.90 % Dox was released from TPPL at pH 5.6 (Figure 14A, the embedded figure focused on the first 4 h). During the first 5 h, burst release was observed with 34.41 ± 1.75 % at pH 7.4 and 57.97 ± 1.20 % at pH 5.6. Then, the sustained release was observed, and after 72 h, TPPL released almost all the encapsulated Dox at pH 5.6 (96.01 ± 1.35 %) whereas 54.79 ± 2.91 % of Dox

was released at pH 7.4 (Figure 14A). There was no statistically significant difference in the amount of Dox released from PPL at pH 7.4 and 5.6 till the 72 h time point. At acidic pH 5.6, 99.60 ± 0.21 % Dox was released from PPL at 96 h whereas 73.50 ± 0.87 % Dox was released at physiological pH 7.4 (Figure 14B).

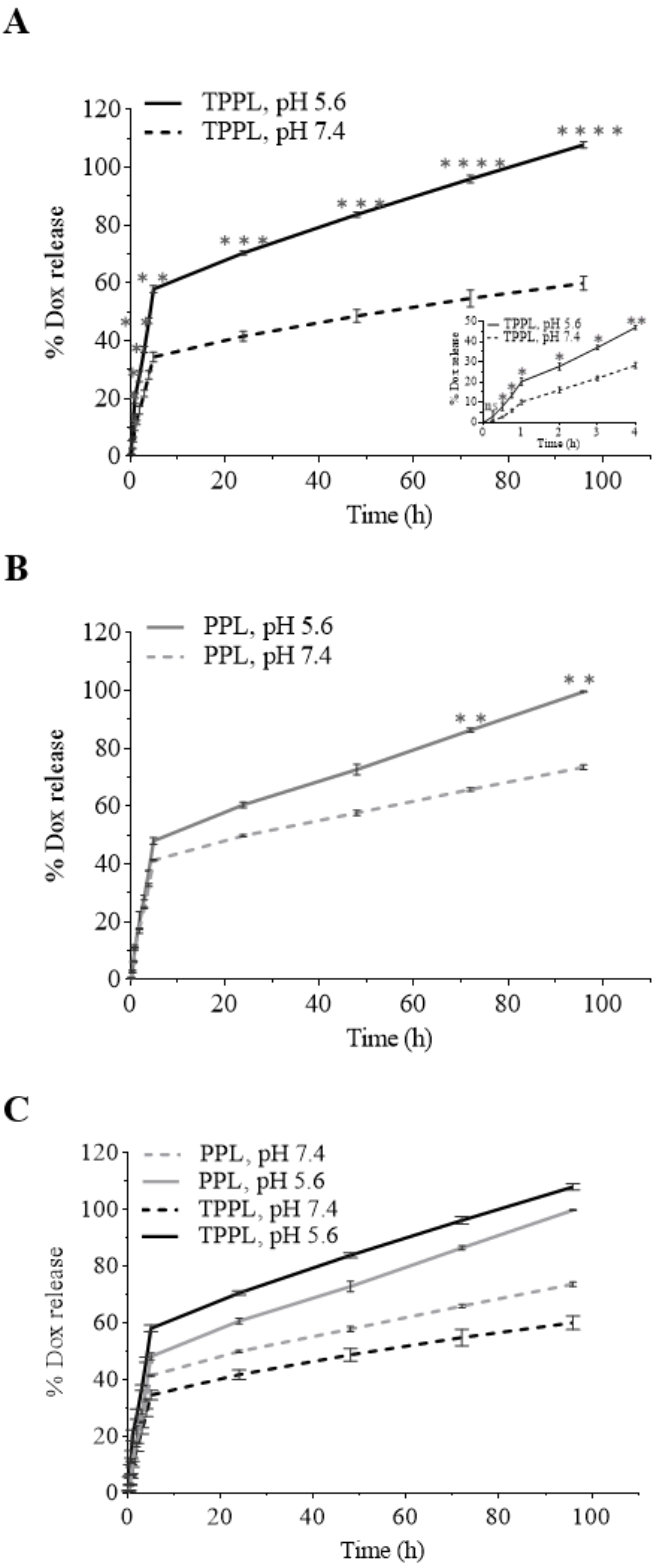

Figure 14. Dox release from A. TPPL, B. PPL in pH 7.4 and 5.6 buffers, and C. Combined release profile. One-way ANOVA using Tukey's multiple comparison tests was conducted for each time point; $p < 0.05$ was accepted as statistically significant.

4.7 Cytotoxicity of Dox-loaded TPPL and PPL

The dose-dependent cytotoxicity of free Dox, Dox-loaded TPPL, and Dox-loaded PPL in HCT116 cells is shown in Figure 15. After 48 h incubation, IC_{50} values of free Dox, Dox-loaded TPPL, and Dox-loaded PPL were 0.55 μM (Figure 15A), 0.34 μM (Figure 15B), and 0.47 μM (Figure 15C), respectively. The IC_{50} value of Dox-loaded TPPL was 1.62-fold lower than that of free Dox and 1.42-fold lower than that of Dox-loaded PPL (Figure 15). The IC_{50} value of Dox-loaded PPL was also 1.17-fold lower than that of free Dox.

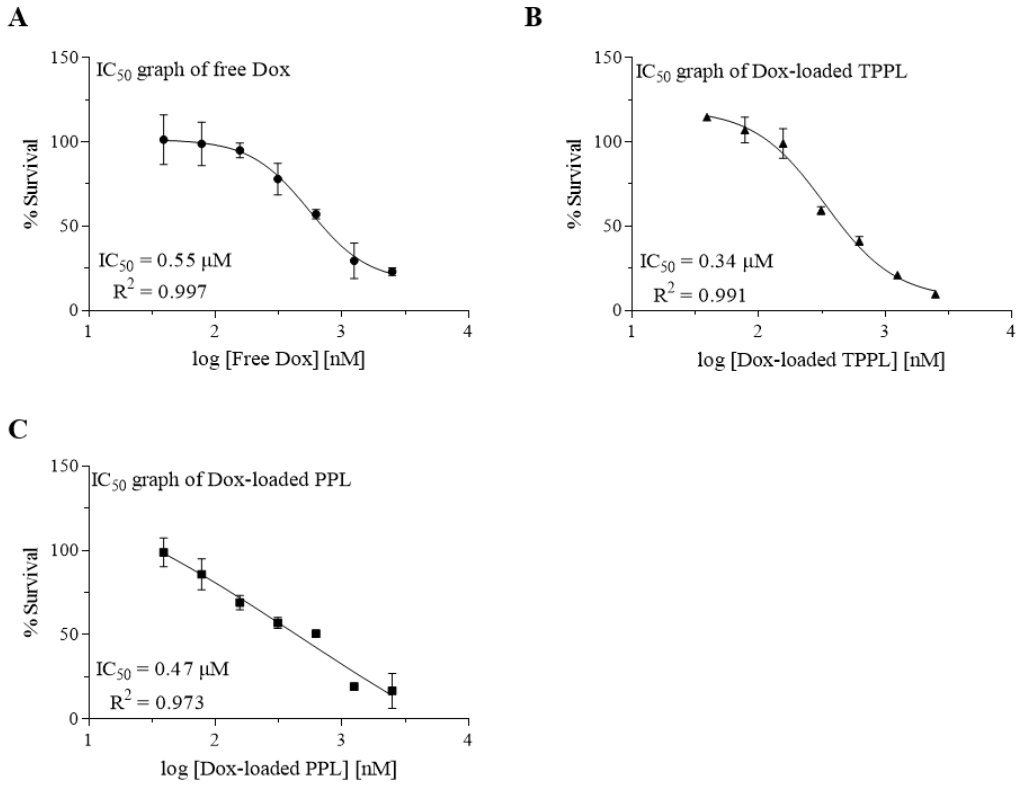

Figure 15. IC_{50} graphs of A. the free Dox, B. Dox-loaded TPPL, and C. Dox-loaded PPL in HCT116 cell lines at 48 h. The graphs were generated using GraphPad Prism 9.3.1 software for IC_{50} calculations based on WST-8 data.

4.8 ROS Levels

The intracellular ROS levels were measured using H_2DCFDA, which is oxidized to highly fluorescent 2',7'-dichlorofluorescein (DCF) in the presence of ROS. The

fluorescence data was normalized to the corresponding cell viability data at 24 h Dox incubation because of the observed cell death at the 24 h post-treatment point. Dox-loaded TPPL showed an increased amount of ROS production in HCT116 cells statistically significantly compared to free Dox and Dox-loaded PPL (Figure 16). The treatment of cells with ROS scavenger NAC together with Dox did not cause a change in ROS levels indicating that an increase in ROS in the cells was due to Dox treatment (Figure 16).

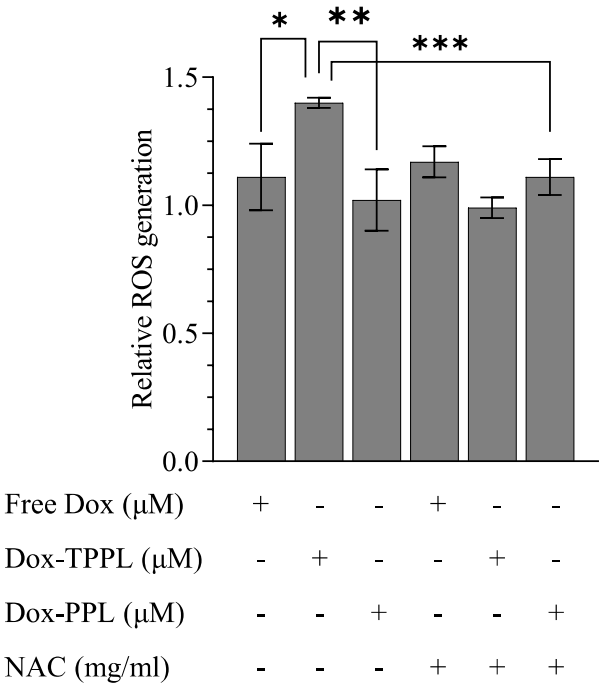

Figure 16. ROS was measured using the H_2DCFDA assay in HCT116 cells treated with free Dox, Dox-loaded PPL, and Dox-loaded TPPL for 24 h and normalized to the corresponding viable cells. Data are shown as mean fold change to untreated control ± STD.

5 DISCUSSION

Metabolically, healthy cells differ from cancer cells. The metabolic pathways of cancer cells are disrupted which leads to unregulated cell growth. The redox reactions are oxygen-consuming metabolic pathways used for cell survival. The mitochondrion, the powerhouse of the cell, is an organelle that contains redox reactions. (90,91). The special bilayer structure of mitochondrion makes it a promising therapeutic target in the diagnosis and treatment of diseases such as cancer, neurodegenerative diseases, and metabolic diseases. Owing to the special structure of a mitochondrion where larger transition pores are included within the OMM, some of the therapeutic molecules can pass through via passive diffusion. However, since the IMM contains smaller transition pores some of the therapeutic molecules cannot arrive through the matrix (58). To overcome such difficulties, mitochondriotropic moieties were developed which provide direct targeting to mitochondria (58,59). In this study, TPP-conjugated amphiphilic DSPE-PEG polymer has been successfully synthesized and used as a mitochondriotropic moiety.

Both mitochondria-targeted and non-targeted liposomes were successfully prepared using thin film hydration method. Due to the adjusted liposomal formulation of Dox-loaded TPPL, it is expected that encapsulated drug molecules will be released at mitochondria and thereby the therapeutic effect of the drug will be enhanced via the mitochondria-targeted liposomal formulation. Additionally, the random interactions of the drug with other organelles will be prevented and therefore off-target effects will be reduced. Also, both non-targeted empty and Dox-loaded PPLs were prepared. The characterization of all liposomal formulations prepared during this study was determined in terms of size, PDI, zeta potential, shape, stability, and encapsulation efficiency. The size of all liposomal formulations is lower than 200 nm, suggesting that they stay longer in circulation and accumulate in the tumor microenvironment more effectively (52). The PDI of all liposomes is below 0.2 indicating that the size distribution of the liposomes is monodisperse (53). The zeta potential of mitochondria-targeted liposomes was positive due to the DSPE-PEG-TPP polymer whereas non-targeted PEGylated liposomes were negatively charged, as expected. According to

characterization based on the physical structure of liposomes, both empty and Dox-loaded liposomes were spherically shaped. However, since TEM images were taken under a high vacuum, water in the aqueous core of the liposomes may evaporate, and thus liposomes may shrink as the water evaporates. Therefore, the size of liposomes obtained in TEM images may be smaller than the size determined in DLS, and a slightly distorted round image may be obtained in TEM (104,105).

The stability of the liposomal formulations depends on both chemical factors such as oxidation of the lipid content and the formation of free radicals in fatty acid tails and physical factors, such as storage temperature and environment (102). Thus, the stability of the liposomes was determined based on the storage temperature. According to the physicochemical properties of both TPPL and PPL were stable at 4 °C. Similarly, Muppidi et al. demonstrated that the stability of PEGylated liposomes based on their size was favorably stable at RT and 4 °C for 3 months but not at 37 °C. Moreover, they observed fungal growth in liposomes stored at 37 °C and RT after a month and 3 months, respectively. Therefore, the only stable temperature condition for liposomes was decided to be 4 °C (106). In this study, cloudiness was seen only in the liposomes stored at 37 °C after 8 weeks. However, no changes were observed in the liposomes stored at RT and 4 °C. Ball and colleagues stated that the PEGylated liposomes stored at 4 °C were stable for more than 150 days compared to other storage conditions which were -20 °C and RT (107).

Since the pH of the tumor tissue is acidic (pH 5.6-6.8) (3,70) the *in vitro* release profile of Dox-loaded TPPL and PPL were analyzed at two different pH; physiological pH 7.4 and acidic pH 5.6 at 37 °C. The concentration of Dox released from both TPPL and PPL was higher at acidic pH 5.6 which indicates that drug release occurs at tumor microenvironment. Although both TPPL and PPL showed an increased release rate at pH 5.6 compared to pH 7.4, the release rate from TPPL was higher than PPL during the first 5 h. Hou et al. also state that there was a pH-dependent drug release profile of Dox. The release rate of Dox from nanoparticles is enhanced as the pH of the medium decreases (68).

The cellular uptake capacity of the fluorescently (RhB) labeled liposomes was demonstrated by confocal microscopy. According to the result obtained after mitochondrial and nuclear staining, it has been seen that DSPE-PEG-TPP-conjugated RhB-labeled liposomes were specifically and effectively localized in the mitochondria whereas non-targeted liposomes were not. Additionally, as the incubation time increased, the intensity of the co-localization at mitochondria was also increased. Even so, the localization time of liposomes varies from study to study since different types of cells, liposomal formulations, and time points were chosen during investigations (1,64,108). Kang and colleagues demonstrated via confocal microscopy that there was an intercellular accumulation of mitochondria-targeted Rh-TPP-DSPE-PEG and Rh-DQA-DSPE-PEG after 1 h of incubation in B16F10 murine melanoma cells (108). Zhou and colleagues reported that internalization into A549 cells and localization at mitochondria of $TPGS_{1000}$-TPP liposomes were observed within 30 min and 24 h, respectively (1)

After that, the cytotoxicity of the empty TPPL and PPL was determined by monitoring the effect of liposomal formulation on the proliferation of HCT116 cells. It has been found that empty liposome formulations were non-toxic to the cells. Similarly, Biswas and colleagues demonstrated that mitochondria-targeted TPP-PEG-L-8% was nontoxic to HeLa cells after 24 h incubation. However, mitochondria-targeted liposome with stearyl residue, STPP-L-8% was found to be toxic starting from 15.63 μg/ml concentration. The toxicity difference between the liposomes was explained by the toxicity of the stearyl moiety (64). Zhou et al. stated that empty $TPGS_{1000}$-TPP liposomes were toxic to A549 cells at concentrations higher than 1 μM and suggested that this cytotoxicity was caused by $TPGS_{1000}$ (1). Moreover, Kang et al. reported that empty TPP-DSPE-PEG and DQA-DSPE-PEG liposomes were not cytotoxic to B16F10 murine melanoma cells (108). Li and colleagues also indicated that empty TPP-PEG liposomes were nontoxic to MDA-MB-231 cells (92). In conclusion, various studies stated that the mitochondria-targeting group, TPP, either by itself or when conjugated with PEG-PE, has no cytotoxic effect on different types of cancer cells (1,64,92,108).

Subsequently, the cytotoxicity of the free Dox, Dox-TPPL, and Dox-PPL was measured against HCT116 cells using CCK-8 assay and corresponding empty liposomes were used as control group. Dose-dependent cytotoxicity was observed after 48 h incubation. All Dox-loaded liposomal formulations exhibited higher cytotoxicity in comparison with free Dox. In addition to this, Dox-loaded TPPL showed lower IC_{50} value compared to free Dox and Dox-loaded PPL. This could be attributed to efficient cellular uptake of Dox-TPPL by cancer cells.

The ROS produced by the Dox-loaded TPPL was statistically significantly higher compared to free Dox and Dox-loaded PPL. Hou et al. also demonstrated that ROS generated by TPP-Dox nanoparticles is higher than that of free Dox in A549 and HeLa cells at each time point (12, 24, 48 h) (68)

Briefly, the cellular uptake capacity, the drug release profile, and the cytotoxicity of liposomes were determined using the optimized liposomal formulations. The cytotoxic effect of empty and Dox-loaded TPPL was compared with empty and Dox-loaded PPL and free Dox. Subsequently, ROS levels were measured after treating HCT116 cells with free Dox, Dox-loaded PPL, and Dox-loaded TPPL. To sum up, in terms of the data constructed throughout this study, the mitochondria-targeted liposomes prepared in this study have the potential to be used in targeting different types of cancer and mitochondrial diseases.

6 CONCLUSION

The mitochondria-targeting polymer, DSPE-PEG-TPP polymer, was successfully synthesized and used for preparing liposomal formulations. The physicochemical properties of both empty and Dox-loaded liposomes, including particle size, PDI, and zeta potential were determined. Also, empty liposomes were found to be stable at 4 ºC for two months. Additionally, for Dox-loaded liposomes, the final concentration of Dox encapsulated into the liposome was measured. Interestingly, the encapsulation efficiency of PPL was higher than that of TPPL. This situation might be caused by the steric hindrance between the molecules. The encapsulation efficiency of TPPL might be decreased since DSPE-PEG-TPP polymer is larger than PEG-PE. The size distribution of liposomes was monodisperse. The surface charge of non-targeted PEGylated liposomes was negative and mitochondria-targeted PEGylated liposomes were positive, as expected. Also, TEM data was obtained to observe the physical characteristics of liposomes and it has been found that all formulations were spherically shaped. The mitochondriotropic activity of TPPL was confirmed by confocal microscopy and it has been proved that targeted liposomes were localized in mitochondria whereas non-targeted liposomes were not. The cellular uptake capacity of Dox-loaded TPPL and PPL was also quantitatively determined via flow cytometry analysis. When the population of unstained cells and treated cells were compared, a shift was observed indicating that Dox-loaded liposomes were successfully internalized within HCT116 cells. Moreover, it has been demonstrated that empty TPPL and PPL were not cytotoxic to HCT116 cells. On the other hand, the cytotoxic effect of Dox-loaded TPPL and PPL was higher than free Dox. Finally, the level of ROS produced through Dox-loaded TPPL-treated HCT116 cells was statistically significantly the highest when compared to free Dox and Dox-loaded PPL treatment. Overall, the results suggest that the DSPE-PEG-TPP polymer conjugated liposomes are promising vehicles for targeted delivery to mitochondria.

7 REFERENCES

1. Zhou J, Zhao WY, Ma X, Ju RJ, Li XY, Li N, et al. The anticancer efficacy of paclitaxel liposomes modified with mitochondrial targeting conjugate in resistant lung cancer. Biomaterials. 2013 May;34(14):3626–38.
2. Moghimipour E, Rezaei M, Ramezani Z, Kouchak M, Amini M, Angali KA, et al. Transferrin targeted liposomal 5-fluorouracil induced apoptosis via mitochondria signaling pathway in cancer cells. Life Sci. 2018 Feb 1;194:104–10.
3. Handali S, Moghimipour E, Rezaei M, Ramezani Z, Kouchak M, Amini M, et al. A novel 5-Fluorouracil targeted delivery to colon cancer using folic acid conjugated liposomes. Biomedicine and Pharmacotherapy. 2018 Dec 1;108:1259–73.
4. Fathi S, Oyelere AK. Liposomal drug delivery systems for targeted cancer therapy: Is active targeting the best choice? Vol. 8, Future Medicinal Chemistry. Future Science; 2016. p. 2091–112.
5. Gullotti E, Yeo Y. Extracellularly activated nanocarriers: A new paradigm of tumor targeted drug delivery. Vol. 6, Molecular Pharmaceutics. 2009. p. 1041–51.
6. Abu Lila AS, Kizuki S, Doi Y, Suzuki T, Ishida T, Kiwada H. Oxaliplatin encapsulated in PEG-coated cationic liposomes induces significant tumor growth suppression via a dual-targeting approach in a murine solid tumor model. Journal of Controlled Release. 2009 Jul 1;137(1):8–14.
7. Yang C, Liu HZ, Fu ZX, Lu WD. Oxaliplatin long-circulating liposomes improved therapeutic index of colorectal carcinoma. BMC Biotechnol. 2011 Mar 15;11.
8. Hamzehzadeh L, Imanparast A, Tajbakhsh A, Rezaee M, Pasdar A. New approaches to use nanoparticles for treatment of colorectal cancer; a brief review. Vol. 1, Nanomedicine Research Journal. Tehran University of Medical Sciences; 2016. p. 59–68.
9. Boddapati S V., D'Souza GGM, Erdogan S, Torchilin VP, Weissig V. Organelle-targeted nanocarriers: Specific delivery of liposomal ceramide to mitochondria enhances its cytotoxicity in vitro and in vivo. Nano Lett. 2008 Aug;8(8):2559–63.
10. Battogtokh G, Cho YY, Lee JY, Lee HS, Kang HC. Mitochondrial-targeting anticancer agent conjugates and nanocarrier systems for cancer treatment. Front Pharmacol. 2018 Apr 1;9.
11. Chen ZP, Li M, Zhang LJ, He JY, Wu L, Xiao YY, et al. Mitochondria-targeted drug delivery system for cancer treatment. Vol. 24, Journal of Drug Targeting. Taylor and Francis Ltd; 2016. p. 492–502.
12. Uhumwangho M, Okor R. Current trends in the production and biomedical applications of liposomes: a review. Journal of Medicine and Biomedical Research. 2005;4(1):9–21.
13. Bangham AD, Horne RW. Negative staining of phospholipids and their structural modification by surface-active agents as observed in the electron microscope. J Mol Biol. 1964;8(5):660–8.
14. Hubbell JA, Chilkoti A. Nanomaterials for drug delivery. Vol. 337, Science. American Association for the Advancement of Science; 2012. p. 303–5.
15. Ventola CL. The nanomedicine revolution: part 1: emerging concepts. P T. 2012 Sep;37(9):512–25.
16. Sessa G, Weissmann G. Phospholipid spherules (liposomes) as a model for biological membranes [Internet]. Available from: www.jlr.org
17. Bozzuto G, Molinari A. Liposomes as nanomedical devices. Vol. 10, International Journal of Nanomedicine. Dove Medical Press Ltd.; 2015. p. 975–99.
18. Sercombe L, Veerati T, Moheimani F, Wu SY, Sood AK, Hua S. Advances and challenges of liposome assisted drug delivery. Vol. 6, Frontiers in Pharmacology. Frontiers Media S.A.; 2015.
19. Sharma D, Ali AAE, Trivedi LR. An Updated Review On:Liposomes as Drug Delivery System. Pharmatutor. 2018 Jan 2;6(2):50.
20. Nisini R, Poerio N, Mariotti S, De Santis F, Fraziano M. The multirole of liposomes in therapy and prevention of infectious diseases. Vol. 9, Frontiers in Immunology. Frontiers Media S.A.; 2018.
21. Liu P, Chen G, Zhang J. A Review of Liposomes as a Drug Delivery System: Current Status of Approved Products, Regulatory Environments, and Future Perspectives. Vol. 27, Molecules. MDPI; 2022.

22. Jiang Y, Li W, Wang Z, Lu J. Lipid-Based Nanotechnology: Liposome. Vol. 16, Pharmaceutics. Multidisciplinary Digital Publishing Institute (MDPI); 2024.
23. Nsairat H, Khater D, Sayed U, Odeh F, Al Bawab A, Alshaer W. Liposomes: structure, composition, types, and clinical applications. Vol. 8, Heliyon. Elsevier Ltd; 2022.
24. Monteiro N, Martins A, Reis RL, Neves NM. Liposomes in tissue engineering and regenerative medicine. Vol. 11, Journal of the Royal Society Interface. Royal Society of London; 2014.
25. van Hoogevest P, Wendel A. The use of natural and synthetic phospholipids as pharmaceutical excipients. Vol. 116, European Journal of Lipid Science and Technology. Wiley-VCH Verlag; 2014. p. 1088–107.
26. Briuglia ML, Rotella C, McFarlane A, Lamprou DA. Influence of cholesterol on liposome stability and on in vitro drug release. Drug Deliv Transl Res. 2015 Jun 1;5(3):231–42.
27. Sivadasan D, Sultan MH, Madkhali OA, Alessa AA, Alsabei SH. Stealth Liposomes (PEGylated) Containing an Anticancer Drug Camptothecin: In Vitro Characterization and In Vivo Pharmacokinetic and Tissue Distribution Study. Molecules. 2022 Feb 1;27(3).
28. Mohamed M, Abu Lila AS, Shimizu T, Alaaeldin E, Hussein A, Sarhan HA, et al. PEGylated liposomes: immunological responses. Vol. 20, Science and Technology of Advanced Materials. Taylor and Francis Ltd.; 2019. p. 710–24.
29. Bulbake U, Doppalapudi S, Kommineni N, Khan W. Liposomal formulations in clinical use: An updated review. Vol. 9, Pharmaceutics. MDPI AG; 2017.
30. Tam YT, To KKW, Chow AHL. Fabrication of doxorubicin nanoparticles by controlled antisolvent precipitation for enhanced intracellular delivery. Colloids Surf B Biointerfaces. 2016 Mar 1;139:249–58.
31. Alfarouk KO, Stock CM, Taylor S, Walsh M, Muddathir AK, Verduzco D, et al. Resistance to cancer chemotherapy: Failure in drug response from ADME to P-gp. Vol. 15, Cancer Cell International. BioMed Central Ltd.; 2015.
32. Guven C, Sevgiler Y, Taskin E. Mitochondrial Dysfunction Associated with Doxorubicin. In: Mitochondrial Diseases. InTech; 2018.
33. Wu B Bin, Leung KT, Poon ENY. Mitochondrial-Targeted Therapy for Doxorubicin-Induced Cardiotoxicity. Vol. 23, International Journal of Molecular Sciences. MDPI; 2022.
34. Jean SR, Tulumello D V., Riganti C, Liyanage SU, Schimmer AD, Kelley SO. Mitochondrial Targeting of Doxorubicin Eliminates Nuclear Effects Associated with Cardiotoxicity. ACS Chem Biol. 2015 Sep 18;10(9):2007–15.
35. Ogawara K ichi, Un K, Tanaka K ichi, Higaki K, Kimura T. In vivo anti-tumor effect of PEG liposomal doxorubicin (DOX) in DOX-resistant tumor-bearing mice: Involvement of cytotoxic effect on vascular endothelial cells. Journal of Controlled Release. 2009 Jan 5;133(1):4–10.
36. Yoshizawa Y, Kono Y, Ogawara KI, Kimura T, Higaki K. PEG liposomalization of paclitaxel improved its in vivo disposition and anti-tumor efficacy. Int J Pharm. 2011 Jun 30;412(1–2):132–41.
37. Gabizon A, Amitay Y, Tzemach D, Gorin J, Shmeeda H, Zalipsky S. Therapeutic efficacy of a lipid-based prodrug of mitomycin C in pegylated liposomes: Studies with human gastro-entero-pancreatic ectopic tumor models. Journal of Controlled Release. 2012 Jun 10;160(2):245–53.
38. Barba AA, Bochicchio S, Dalmoro A, Lamberti G. Lipid delivery systems for nucleic-acid-based-drugs: From production to clinical applications. Vol. 11, Pharmaceutics. MDPI AG; 2019.
39. Zhang JX, Wang K, Mao ZF, Fan X, Jiang DL, Chen M, et al. Application of liposomes in drug development - focus on gastroenterological targets. Vol. 8, International Journal of Nanomedicine. 2013. p. 1325–34.
40. Wu H, Yu M, Miao Y, He S, Dai Z, Song W, et al. Cholesterol-tuned liposomal membrane rigidity directs tumor penetration and anti-tumor effect. Acta Pharm Sin B. 2019 Jul 1;9(4):858–70.
41. Torchilin VP. Recent advances with liposomes as pharmaceutical carriers. Vol. 4, Nature Reviews Drug Discovery. 2005. p. 145–60.
42. Lu L, Ding Y, Zhang Y, Ho RJY, Zhao Y, Zhang T, et al. Antibody-modified liposomes for tumor-targeting delivery of timosaponin AIII. Int J Nanomedicine. 2018 Mar 29;13:1927–44.
43. Lee Y, Thompson DH. Stimuli-responsive liposomes for drug delivery. Vol. 9, Wiley Interdisciplinary Reviews: Nanomedicine and Nanobiotechnology. Wiley-Blackwell; 2017.
44. Soares DCF, De Oliveira MC, De Barros ALB, Cardoso VN, Ramaldes GA. Liposomes radiolabeled with 159Gd: In vitro antitumoral activity, biodistribution study and scintigraphic

image in Ehrlich tumor bearing mice. European Journal of Pharmaceutical Sciences. 2011 Jul 17;43(4):290–6.
45. Pande S. Liposomes for drug delivery: review of vesicular composition, factors affecting drug release and drug loading in liposomes. Vol. 51, Artificial Cells, Nanomedicine and Biotechnology. Taylor and Francis Ltd.; 2023. p. 428–40.
46. Gubernator J. Active methods of drug loading into liposomes: Recent strategies for stable drug entrapment and increased in vivo activity. Vol. 8, Expert Opinion on Drug Delivery. 2011. p. 565–80.
47. Akbarzadeh A, Rezaei-Sadabady R, Davaran S, Joo SW, Zarghami N, Hanifehpour Y, et al. Liposome: Classification, preparation, and applications. Nanoscale Res Lett. 2013;8(1).
48. Yang S, Chen J, Zhao D, Han D, Chen X. Comparative study on preparative methods of DC-Chol/DOPE liposomes and formulation optimization by determining encapsulation efficiency. Int J Pharm. 2012 Sep 15;434(1–2):155–60.
49. Tomnikova A, Orgonikova A, Krizek T. Liposomes: preparation and characterization with a special focus on the application of capillary electrophoresis. Monatshefte fur Chemie. Springer; 2022.
50. Castañeda-Reyes ED, Perea-Flores M de J, Davila-Ortiz G, Lee Y, de Mejia EG. Development, characterization and use of liposomes as amphipathic transporters of bioactive compounds for melanoma treatment and reduction of skin inflammation: A review. Vol. 15, International Journal of Nanomedicine. Dove Medical Press Ltd; 2020. p. 7627–50.
51. Surianarayanan R, Gurumallappa Shivakumar H, Varma Vegesna NSK, Srivastava A. Effect of sample Concentration on the Characterization of Liposomes using Dynamic light Scattering Technique. Pharm Methods. 2016 Jan 1;7(1):70–4.
52. Andra VVSNL, Pammi SVN, Bhatraju LVKP, Ruddaraju LK. A Comprehensive Review on Novel Liposomal Methodologies, Commercial Formulations, Clinical Trials and Patents. Vol. 12, BioNanoScience. Springer; 2022. p. 274–91.
53. Soema PC, Willems GJ, Jiskoot W, Amorij JP, Kersten GF. Predicting the influence of liposomal lipid composition on liposome size, zeta potential and liposome-induced dendritic cell maturation using a design of experiments approach. European Journal of Pharmaceutics and Biopharmaceutics. 2015 Jul 10;94:427–35.
54. Smith MC, Crist RM, Clogston JD, McNeil SE. Zeta potential: a case study of cationic, anionic, and neutral liposomes. Anal Bioanal Chem. 2017 Sep 1;409(24):5779–87.
55. Németh Z, Csóka I, Semnani Jazani R, Sipos B, Haspel H, Kozma G, et al. Quality by Design-Driven Zeta Potential Optimisation Study of Liposomes with Charge Imparting Membrane Additives. Pharmaceutics. 2022 Sep 1;14(9).
56. Edwards KA, Baeumner AJ. Analysis of liposomes. Vol. 68, Talanta. Elsevier; 2006. p. 1432–41.
57. Wongrakpanich A, Geary SM, Joiner MLA, Anderson ME, Salem AK. Mitochondria-targeting particles. Vol. 9, Nanomedicine. Future Medicine Ltd.; 2014. p. 2531–43.
58. Wang Z, Guo W, Kuang X, Hou S, Liu H. Nanopreparations for mitochondria targeting drug delivery system: Current strategies and future prospective. Vol. 12, Asian Journal of Pharmaceutical Sciences. Shenyang Pharmaceutical University; 2017. p. 498–508.
59. Kalyanaraman B, Cheng G, Hardy M, Ouari O, Lopez M, Joseph J, et al. A review of the basics of mitochondrial bioenergetics, metabolism, and related signaling pathways in cancer cells: Therapeutic targeting of tumor mitochondria with lipophilic cationic compounds. Vol. 14, Redox Biology. Elsevier B.V.; 2018. p. 316–27.
60. Wang F, Ogasawara MA, Huang P. Small mitochondria-targeting molecules as anti-cancer agents. Vol. 31, Molecular Aspects of Medicine. 2010. p. 75–92.
61. Zielonka J, Joseph J, Sikora A, Hardy M, Ouari O, Vasquez-Vivar J, et al. Mitochondria-Targeted Triphenylphosphonium-Based Compounds: Syntheses, Mechanisms of Action, and Therapeutic and Diagnostic Applications. Vol. 117, Chemical Reviews. American Chemical Society; 2017. p. 10043–120.
62. He H, Li DW, Yang LY, Fu L, Zhu XJ, Wong WK, et al. A novel bifunctional mitochondria-targeted anticancer agent with high selectivity for cancer cells. Sci Rep. 2015 Sep 4;5.
63. Patel NR, Hatziantoniou S, Georgopoulos A, Demetzos C, Torchilin VP, Weissig V, et al. Mitochondria-targeted liposomes improve the apoptotic and cytotoxic action of sclareol. J Liposome Res. 2010 Sep;20(3):244–9.

64. Biswas S, Dodwadkar NS, Deshpande PP, Torchilin VP. Liposomes loaded with paclitaxel and modified with novel triphenylphosphonium-PEG-PE conjugate possess low toxicity, target mitochondria and demonstrate enhanced antitumor effects in vitro and in vivo. Journal of Controlled Release. 2012 May 10;159(3):393–402.
65. Chamberlain GR, Tulumello D V., Kelley SO. Targeted delivery of doxorubicin to mitochondria. ACS Chem Biol. 2013 Jul 19;8(7):1389–95.
66. Cui H, Huan M lei, Ye W liang, Liu D zhou, Teng Z hui, Mei QB, et al. Mitochondria and Nucleus Dual Delivery System To Overcome DOX Resistance. Mol Pharm. 2017 Mar 6;14(3):746–56.
67. Han M, Vakili MR, Soleymani Abyaneh H, Molavi O, Lai R, Lavasanifar A. Mitochondrial delivery of doxorubicin via triphenylphosphine modification for overcoming drug resistance in MDA-MB-435/DOX cells. Mol Pharm. 2014 Aug 4;11(8):2640–9.
68. Hou J, Yu X, Shen Y, Shi Y, Su C, Zhao L. Triphenyl Phosphine-Functionalized Chitosan Nanoparticles Enhanced Antitumor Efficiency Through Targeted Delivery of Doxorubicin to Mitochondria. Nanoscale Res Lett. 2017 Dec 1;12(1).
69. Khatun Z, Choi YS, Kim YG, Yoon K, Nurunnabi M, Li L, et al. Bioreducible Poly(ethylene glycol)–Triphenylphosphonium Conjugate as a Bioactivable Mitochondria-Targeting Nanocarrier. Biomacromolecules [Internet]. 2017 Apr 10;18(4):1074–85. Available from: https://doi.org/10.1021/acs.biomac.6b01324
70. Liu H na, Guo N ning, Guo W wei, Huang-Fu M yi, Vakili MR, Chen J jian, et al. Delivery of mitochondriotropic doxorubicin derivatives using self-assembling hyaluronic acid nanocarriers in doxorubicin-resistant breast cancer. Acta Pharmacol Sin. 2018 Oct 1;39(10):1681–92.
71. Xiong H, Du S, Ni J, Zhou J, Yao J. Mitochondria and nuclei dual-targeted heterogeneous hydroxyapatite nanoparticles for enhancing therapeutic efficacy of doxorubicin. Biomaterials. 2016 Jul 1;94:70–83.
72. Baracca A, Sgarbi G, Solaini G, Lenaz G. Rhodamine 123 as a probe of mitochondrial membrane potential: Evaluation of proton flux through F0 during ATP synthesis. Biochim Biophys Acta Bioenerg. 2003 Sep 30;1606(1–3):137–46.
73. Biswas S, Dodwadkar NS, Sawant RR, Koshkaryev A, Torchilin VP. Surface modification of liposomes with rhodamine-123-conjugated polymer results in enhanced mitochondrial targeting. J Drug Target. 2011 Aug;19(7):552–61.
74. Fantin VR, Berardi MJ, Scorrano L, Korsmeyer SJ, Leder P. A novel mitochondriotoxic small molecule that selectively inhibits tumor cell growth.
75. Dubinin M V., Semenova AA, Ilzorkina AI, Penkov N V., Nedopekina DA, Sharapov VA, et al. Mitochondria-targeted prooxidant effects of betulinic acid conjugated with delocalized lipophilic cation F16. Free Radic Biol Med. 2021 May 20;168:55–69.
76. Li X, Srinivasan SR, Connarn J, Ahmad A, Young ZT, Kabza AM, et al. Analogues of the allosteric heat shock protein 70 (Hsp70) inhibitor, MKT-077, as anti-cancer agents. ACS Med Chem Lett. 2013 Nov 14;4(11):1042–7.
77. Byoung HK, Plescia J, Ho YS, Meli M, Colombo G, Beebe K, et al. Combinatorial drug design targeting multiple cancer signaling networks controlled by mitochondrial Hsp90. Journal of Clinical Investigation. 2009 Mar 2;119(3):454–64.
78. Weiss MJ, Wong JR, Ha S, Bledaytt R, Salemt RR, Steele GD, et al. Dequalinium, a topical antimicrobial agent, displays anticarcinoma activity based on selective mitochondrial accumulation (rhodamine 123/cyanine/chemotherapy/lipophilic/cationic). Vol. 84, Medical Sciences. 1987.
79. Wang H, Yin H, Yan F, Sun M, Du L, Peng W, et al. Folate-mediated mitochondrial targeting with doxorubicin-polyrotaxane nanoparticles overcomes multidrug resistance [Internet]. Vol. 6, Oncotarget. 2014. Available from: www.impactjournals.com/oncotarget/
80. Sun Y, Yang Q, Xia X, Li X, Ruan W, Zheng M, et al. Polymeric Nanoparticles for Mitochondria Targeting Mediated Robust Cancer Therapy. Vol. 9, Frontiers in Bioengineering and Biotechnology. Frontiers Media S.A.; 2021.
81. Sun Y, Zhang H, Lu G, Wang H, Lu Y, Fan L. Mitochondria-targeted cancer therapy based on functional peptides. Chinese Chemical Letters. 2023 May 1;34(5).
82. Kim S, Nam HY, Lee J, Seo J. Mitochondrion-Targeting Peptides and Peptidomimetics: Recent Progress and Design Principles. Vol. 59, Biochemistry. American Chemical Society; 2020. p. 270–84.

83. Mallick S, Thuy LT, Lee S, Park JI, Choi JS. Liposomes containing cholesterol and mitochondria-penetrating peptide (MPP) for targeted delivery of antimycin A to A549 cells. Colloids Surf B Biointerfaces. 2018 Jan 1;161:356–64.
84. Lin R, Zhang P, Cheetham AG, Walston J, Abadir P, Cui H. Dual peptide conjugation strategy for improved cellular uptake and mitochondria targeting. Bioconjug Chem. 2015 Jan 21;26(1):71–7.
85. Heller A, Brockhoff G, Goepferich A. Targeting drugs to mitochondria. Vol. 82, European Journal of Pharmaceutics and Biopharmaceutics. 2012. p. 1–18.
86. Ding XW, Robinson M, Li R, Aldhowayan H, Geetha T, Babu JR. Mitochondrial dysfunction and beneficial effects of mitochondria-targeted small peptide SS-31 in Diabetes Mellitus and Alzheimer's disease. Vol. 171, Pharmacological Research. Academic Press; 2021.
87. Szeto HH, Schiller PW. Novel therapies targeting inner mitochondrial membrane-from discovery to clinical development. Vol. 28, Pharmaceutical Research. 2011. p. 2669–79.
88. Szeto HH. First-in-class cardiolipin-protective compound as a therapeutic agent to restore mitochondrial bioenergetics. 2013; Available from: http://dx.doi.org/10.1111/bph.2014.171.issue-8
89. Lyu Y, Xiao Q, Li Y, Wu Y, He W, Yin L. "Locked" cancer cells are more sensitive to chemotherapy. Bioeng Transl Med. 2019 May;4(2).
90. Zhu Y, Dean AE, Horikoshi N, Heer C, Spitz DR, Gius D. Emerging evidence for targeting mitochondrial metabolic dysfunction in cancer therapy. Vol. 128, Journal of Clinical Investigation. American Society for Clinical Investigation; 2018. p. 3682–91.
91. Liberti M V., Locasale JW. The Warburg Effect: How Does it Benefit Cancer Cells? Vol. 41, Trends in Biochemical Sciences. Elsevier Ltd; 2016. p. 211–8.
92. Li WQ, Wang Z, Hao S, He H, Wan Y, Zhu C, et al. Mitochondria-Targeting Polydopamine Nanoparticles to Deliver Doxorubicin for Overcoming Drug Resistance. ACS Appl Mater Interfaces. 2017 May 24;9(20):16793–802.
93. Yingchoncharoen P, Kalinowski DS, Richardson DR. Lipid-based drug delivery systems in cancer therapy: What is available and what is yet to come. Pharmacol Rev. 2016 Jul 1;68(3):701–87.
94. Fang J, Nakamura H, Maeda H. The EPR effect: Unique features of tumor blood vessels for drug delivery, factors involved, and limitations and augmentation of the effect. Vol. 63, Advanced Drug Delivery Reviews. 2011. p. 136–51.
95. Yang T, Cui F De, Choi MK, Lin H, Chung SJ, Shim CK, et al. Liposome formulation of paclitaxel with enhanced solubility and stability. Drug Deliv. 2007 Jun;14(5):301–8.
96. Guzman-Villanueva D, Ryan Mendiola M, Xuan Nguyen H, Weissig V. Influence of Triphenylphosphonium (TPP) Cation Hydrophobization with Phospholipids on Cellular Toxicity and Mitochondrial Selectivity [Internet]. 2015. Available from: www.symbiosisonline.orgwww.symbiosisonlinepublishing.com
97. Nam JH, Kim SY, Seong H. Investigation on Physicochemical Characteristics of a Nanoliposome-Based System for Dual Drug Delivery. Nanoscale Res Lett. 2018;13.
98. Tefas LR, Sylvester B, Tomuta I, Sesarman A, Licarete E, Banciu M, et al. Development of antiproliferative long-circulating liposomes co-encapsulating doxorubicin and curcumin, through the use of a quality-by-design approach. Drug Des Devel Ther. 2017 May 25;11:1605–21.
99. Vila-Caballer M, Codolo G, Munari F, Malfanti A, Fassan M, Rugge M, et al. A pH-sensitive stearoyl-PEG-poly(methacryloyl sulfadimethoxine)-decorated liposome system for protein delivery: An application for bladder cancer treatment. Journal of Controlled Release. 2016 Sep 28;238:31–42.
100. Somuncu B, Ekmekcioglu A, Antmen FM, Ertuzun T, Deniz E, Keskin N, et al. Targeting mitochondrial DNA polymerase gamma for selective inhibition of MLH1 deficient colon cancer growth. PLoS One. 2022 Jun 1;17(6 June).
101. Che J, Okeke C, Hu ZB, Xu J. DSPE-PEG: A Distinctive Component in Drug Delivery System. Curr Pharm Des. 2015 Feb 20;21(12):1598–605.
102. Pasarin D, Ghizdareanu AI, Enascuta CE, Matei CB, Bilbie C, Paraschiv-Palada L, et al. Coating Materials to Increase the Stability of Liposomes. Vol. 15, Polymers. MDPI; 2023.
103. Ibrahim M, Abuwatfa WH, Awad NS, Sabouni R, Husseini GA. Encapsulation, Release, and Cytotoxicity of Doxorubicin Loaded in Liposomes, Micelles, and Metal-Organic Frameworks: A Review. Vol. 14, Pharmaceutics. MDPI; 2022.

104. Mohan A, Narayanan S, Sethuraman S, Krishnan UM. Novel resveratrol and 5-fluorouracil coencapsulated in PEGylated nanoliposomes improve chemotherapeutic efficacy of combination against head and neck squamous cell carcinoma. Biomed Res Int. 2014;2014.
105. Monnier CA, Thévenaz DC, Balog S, Fiore GL, Vanhecke D, Rothen-Rutishauser B, et al. A guide to investigating colloidal nanoparticles by cryogenic transmission electron microscopy: Pitfalls and benefits. AIMS Biophys. 2015;2(3):245–58.
106. Muppidi K, Pumerantz AS, Wang J, Betageri G. Development and Stability Studies of Novel Liposomal Vancomycin Formulations. ISRN Pharm. 2012 Jan 26;2012:1–8.
107. Lball R, Bajaj P, Whitehead KA. Achieving long-term stability of lipid nanoparticles: Examining the effect of pH, temperature, and lyophilization. Int J Nanomedicine. 2017;12:305–15.
108. Kang JH, Ko YT. Enhanced subcellular trafficking of resveratrol using mitochondriotropic liposomes in cancer cells. Pharmaceutics. 2019 Aug 1;11(8).

8 APPENDIX

APPENDIX 1 – The stability data: Changes in size and PDI based on 4 °C

	Size		PDI	
Week	**TPPL**	**PPL**	**TPPL**	**PPL**
1	132.42 ± 1.40	112.20 ± 4.47	0.18 ± 0.02	0.20 ± 0.01
2	132.90 ± 0.96	108.55 ± 2.33	0.18 ± 0.01	0.20 ± 0.02
3	133.62 ± 3.30	104.18 ± 7.45	0.18 ± 0.01	0.20 ± 0.01
4	134.26 ± 3.01	102.36 ± 3.89	0.19 ± 0.01	0.19 ± 0.02
5	135.01 ± 2.20	101.47 ± 2.38	0.18 ± 0.02	0.20 ± 0.01
6	137.10 ± 4.21	103.27 ± 3.01	0.17 ± 0.00	0.20 ± 0.01
7	135.21 ± 1.19	102.73 ± 4.19	0.17 ± 0.01	0.20 ± 0.01
8	135.05 ± 2.05	104.83 ± 3.34	0.17 ± 0.02	0.19 ± 0.02

APPENDIX 2 – The stability data: Changes in size and PDI based on room temperature

	Size		PDI	
Week	**TPPL**	**PPL**	**TPPL**	**PPL**
1	132.12 ± 0.50	110.47 ± 1.17	0.18 ± 0.01	0.20 ± 0.01
2	133.05 ± 1.66	102.49 ± 0.55	0.17 ± 0.02	0.22 ± 0.01
3	135.03 ± 2.65	107.34 ± 1.98	0.17 ± 0.01	0.23 ± 0.01
4	133.68 ± 1.10	106.28 ± 1.23	0.18 ± 0.00	0.23 ± 0.01
5	133.60 ± 2.36	106.85 ± 1.57	0.17 ± 0.02	0.23 ± 0.01
6	133.39 ± 0.54	108.25 ± 2.32	0.16 ± 0.02	0.23 ± 0.01
7	133.46 ± 0.62	108.35 ± 1.92	0.17 ± 0.02	0.21 ± 0.01
8	132.89 ± 1.11	106.71 ± 3.10	0.17 ± 0.02	0.20 ± 0.03

APPENDIX 3 – The stability data: Changes in size and PDI based on 37 °C

	Size		PDI	
Week	**TPPL**	**PPL**	**TPPL**	**PPL**
1	158.16 ± 1.15	110.23 ± 5.63	0.25 ± 0.01	020 ± 0.01
2	205.93 ± 12.66	104.65 ± 11.16	0.26 ± 0.01	0.19 ± 0.01
3	228.88 ± 22.04	102.94 ± 5.82	0.27 ± 0.03	0.18 ± 0.01
4	241.26 ± 27.40	99.63 ± 1.01	0.27 ± 0.04	0.19 ± 0.01
5	201.46 ± 13.11	100.35 ± 0.83	0.23 ± 0.07	0.18 ± 0.00
6	155.93 ± 9.10	98.92 ± 0.91	0.26 ± 0.01	0.19 ± 0.02
7	198.28 ± 8.66	99.81 ± 2.49	0.23 ± 0.07	0.19 ± 0.01
8	212.64 ± 40.54	98.79 ± 2.00	0.24 ± 0.03	0.19 ± 0.01

APPENDIX 4 – The stability data: Changes in zeta potential based on temperature

4 °C		
Month	**TPPL**	**PPL**
0	6.50 ± 0.17	-13.20 ± 0.30
1	6.90 ± 0.10	-13.10 ± 0.17
2	7.53 ± 0.32	-12.67 ± 0.58
RT		
Month	**TPPL**	**PPL**
0	6.07 ± 0.32	-15.17 ± 0.23
1	2.00 ± 0.17	-16.00 ± 0.46
2	1.10 ± 0.20	-14.63 ± 0.42
37 °C		
Month	**TPPL**	**PPL**
0	5.77 ± 0.15	-13.43 ± 0.64
1	-5.00 ± 0.10	-13.03 ± 0.65
2	-5.73 ± 0.25	-10.10 ± 0.52

APPENDIX 5 – Cumulative percent drug release data

	pH 5.6		pH 7.4	
Time (h)	**TPPL**	**PPL**	**TPPL**	**PPL**
0.25	3.08 ± 2.50	0.66 ± 0.30	0.81 ± 0.18	0.60 ± 0.21
0.5	7.94 ± 1.95	2.81 ± 0.49	2.81 ± 0.27	2.74 ± 0.45
0.75	13.58 ± 1.36	6.17 ± 0.36	5.94 ± 0.76	6.49 ± 0.24
1	20.23 ± 1.90	10.71 ± 0.44	10.09 ± 1.08	11.40 ± 0.55
2	27.76 ± 1.78	19.83 ± 3.76	16.02 ± 1.43	17.63 ± 0.28
3	37.08 ± 1.06	28.41 ± 0.81	21.90 ± 1.10	24.96 ± 0.30
4	46.98 ± 0.97	37.71 ± 0.19	28.26 ± 1.38	32.78 ± 0.58
5	57.97 ± 1.20	48.00 ± 1.25	34.41 ± 1.75	41.36 ± 0.32
24	70.41 ± 0.78	60.58 ± 1.06	41.62 ± 1.70	49.89 ± 0.40
48	83.71 ± 0.91	72.72 ± 1.85	48.67 ± 2.26	57.75 ± 0.87
72	96.02 ± 1.35	86.36 ± 0.69	54.78 ± 2.91	65.84 ± 0.65
96	107.89 ± 1.16	99.60 ± 0.21	59.98 ± 2.46	73.50 ± 0.87

9 CURRICULUM VITAE